Composite Structures 273 (2021) 114322

Contents lists available at ScienceDirect

Composite Structures

journal homepage: www.elsevier.com/locate/compstruct

Diagnosis of NSM FRP reinforcement in concrete by using mixed-effects models and EMI approaches

Ricardo Perera [a,*], Alberto Gil [a], Lluis Torres [b], Cristina Barris [b]

[a] Department of Mechanical Engineering, Technical University of Madrid, c/ José Gutiérrez Abascal, 2, Madrid 28006, Spain
[b] Analysis and Advanced Materials for Structural Design (AMADE), Polytechnic School, University of Girona, Campus Montilivi, Girona 17003, Spain

ARTICLE INFO

Keywords:
NSM-FRP strengthening
Mixed effects models
Structural health monitoring
PZT sensors
Electro-mechanical impedance

ABSTRACT

The use of fibre reinforced polymer (FRP) in civil construction applications with near-surface mounted (NSM) method has gained considerable popularity worldwide as suitable method for strengthening existing concrete structures. However, there is very little experience in the implementation of methods able to give a reliable prediction about the health of this type of structures even although sudden and brittle failure modes are likely to happen. Because of it, more contributions on this topic are really needed in order to prevent possible catastrophic failures. In this paper, a novel approach based on linear mixed effects models implemented on results from experimental tests performed on concrete beams strengthened with NSM FRP has been explored. In spite of their rapid growth in other areas, mixed effects models have barely been applied in structural problems. Impedance measurements captured from PZT sensors embedded and externally bonded to the beam are used for the quantitative and qualitative analysis. This research shows that the evolution of the progressive damage for this kind of repairing method can be effectively monitored using the proposed approach.

1. Introduction

Strengthening of concrete structures with fiber-reinforced polymers (FRPs) plates externally bonded (EB) onto concrete surface is more and more usual [1–3]. Another alternative technique to strengthen concrete beams consists on inserting FRP rods into grooves on concrete covers; this technique is named near surface method (NSM). NSM-FRP technique has some advantages compared to the EB FRP method, such as a better bond performance and better protection to accidental damages as those due to, for instance, vandalism and environmental effects [4–6].

Various failure modes have been identified for NSM FRP strengthened concrete members. In addition to the conventional failures due to concrete crushing and FRP rupture, debonding failures due to the loss of composite action at FRP-adhesive-concrete substrate interfaces or by separation of the concrete cover, play an important role [4–6]. These last failure modes occur in a sudden a brittle way. The implementation of a damage identification methodology able to detect damage in the earliest stages appears to be a very needed and challenging strategy with the purpose of avoiding possible catastrophic and sudden failures and it is the main purpose of this work.

One of the characteristics of the damage we want to identify is that it is very localized and little severe. Conventional vibration-based techniques have been successfully applied for structural health monitoring in other applications [7–9] or even in concrete beams strengthened with NSM-FRP rods [10]; in this case, modal properties such as natural frequencies and mode shapes are used for damage identification. However, due to the non-local nature of these modal properties, their use to detect successfully local minor damage is unsuitable. Furthermore, the use of smart materials capable of providing autonomous, real-time, wireless, reliable and cost effective monitoring is more and more demanded by SHM engineers. Therefore, two issues must be solved for our purposes. The first one is related with the choice of the type of sensor and the suitable physical quantity to be monitored while the second one is concerned with the definition of the damage metric dependent on the monitored signal and the procedure of categorization of the structural modifications once the metric has been chosen.

In the last decades, the use of piezoelectric transducers (PTs) and the electromechanical impedance (EMI) active sensing technique have emerged as attractive tools for the implementation of an online monitoring system [11–14]. Piezoelectric materials are smart materials due to their sensing and actuating properties and some of their advantages lie in their non-invasive nature, the capability of collecting high

* Corresponding author.
E-mail address: ricardo.perera@upm.es (R. Perera).

https://doi.org/10.1016/j.compstruct.2021.114322
Received 30 June 2020; Revised 19 June 2021; Accepted 28 June 2021
Available online 02 July 2021

frequency information in real time and the possibility for a wireless mobile survey configuration [15]. The EMI technique, based on the piezoelectric or electromechanical coupling effects, has shown a great potential in the field of monitoring. On one hand, the host structure can be excited by means of vibrations originated by the application of an electric field in the PT. But, in the same way, the mechanical and geometrical parameters of a PT are coupled electromechanically with the host structure in such a way that the mechanical properties of a structure and, therefore, its possible damage, can be captured using the electric impedance response of PTs coupled to the structure.

By analyzing the electric impedance variation of the piezoelectric sensors in different frequency intervals along the monitoring process the structural damage can be investigated. For it, suitable metrics able to identify variations on the electrical signatures are needed. However, it is also needed the development of methodologies able to discriminate variations in the metrics due to damage of other effects which might cause variations too since not all the changes in the electrical impedances can be attributed to mechanical damage; this interpretation might lead to a mistaken analysis of the problem. Additionally, in case of damage, these methods should be able to perform a categorization of the structural modifications in terms of severity.

Linear Mixed-effects Models (LMMs), also known as multilevel or random effects models, are becoming increasingly popular as a data analysis method [16,17]. The use of LMMs is set to dominate statistical analyses in psychological science and medical sciences [18] and may become the default approach in the future to analyzing quantitative data in different areas, such as SHM. These models can be considered as a generalization of the classic regression approach which includes, along with the usual explanatory variables called fixed effects, also random effects accounting for data auto-correlation and independent random error. Their application is suitable to analyze data collected during a multi-stage or multilevel sampling or repeated measures design, such as those obtained from a continuous monitoring of a structure. The correlations between the different conditions and, therefore, the evolution of the possible structural damage and other phenomena might be captured with LMMs.

In spite of its potential and numerous applications [19–21], to the knowledge of the authors, LMMs have hardly ever been applied to SHM problems and, of course, never for NSM-FRP strengthened structures, where the contributions involving SHM are very few [10,22].

In this work, NSM-FRP strengthened concrete beams subjected to progressive damage stages and instrumented with PTs of different types and bonded in different locations are analyzed. There is an important knowledge gap concerning the amount of information provided by the different proximal sensors for estimating the damage as well as the best suited statistical approach to be applied for fulfilling the task. With this purpose, the objective of this work is to evaluate the single or combined contribution of proximal sensing information provided by EMI data in estimating minor damage in NSM-FRP strengthened concrete beams by using a LMM approach.

This paper is organized as follows. To begin, a review of the EMI method for structural damage identification and the definition of the damage metrics are introduced. The formulation of the linear mixed effects model for our problem is illustrated in Section 3. The description of the experimental tests and the impedance datasets obtained from them are carried out in Section 4. This section describes also in detail the analysis of results performed with the proposed approach. Finally, in the last section, conclusions are presented.

2. Electromechanical impedance

Although EMI method can be implemented experimentally, its modeling is a more complex task. As commented in the introduction, PTs present electrical and mechanical properties which are coupled by the electromechanical phenomenon. A coupling analysis should capture suitably the complex coupling that exists between the mechanical behavior of the structure and the electrical behavior of the transducer. This way, it might be fully explained why structural damage can be detected from the EMI spectrum of the sensor. The analysis methods should be able to make an explicit prediction of the admittance and impedance as it is to be measured in the impedance analyzer connected to the transducer. The implementation of this relationship is necessary to be able to perform a critical analysis of the experimental results obtained.

The model of PT-structure electromechanical interaction in 1D and 2D structure proposed by Liang et al. [23], Xu et al. [24] and Bhalla et al. [25] is frequently used for this purpose.

A PT satisfies the properties of electrical circuits. The electrical admittance $Y(\omega)$ of a PT represents the relation between the output current $I_0(\omega)$ and its excitation voltage $V(\omega)$ and is the inverse of the electromechanical impedance $Z(\omega)$

$$Y(\omega) = \frac{I_0(\omega)}{V(\omega)} = \frac{1}{Z(\omega)} = G(\omega) + jB(\omega) \tag{1}$$

where ω is the input frequency and the admittance has been decomposed in a real part or conductance, G, and an imaginary part or susceptance, B. Usually, the conductance is preferred to identify mechanical variations of a structure to the susceptance, which shows low sensitivity to structural modifications [26,27].

The one-dimensional simple model proposed by Liang et al [23] allows to represent the relation between the electro-mechanical admittance of a piezo-transducer bonded to a structure and the mechanical impedance of the structure, $Z_s(\omega)$, as follows

$$Y(\omega) = j\omega \frac{wl}{h}\left(\bar{\varepsilon}_{33}^{T} - \frac{Z_s(\omega)}{Z_s(\omega) + Z_a(\omega)} d_{3x}^2 \hat{Y}_{xx}^{E}\right) \tag{2}$$

where w, l and h denote the width, length and thickness of the PT patch, respectively; d_{3x}^2 and $\hat{Y}_{xx}^{E}$ are the piezoelectric coupling constant and complex Young's modulus of the PT, respectively, and $\bar{\varepsilon}_{33}^{T} = \varepsilon_{33}^{T}(1 - \delta j)$ is the complex dielectric constant of a PT patch under constant stress, where δ is the dielectric loss factor. Finally, $Z_a(\omega)$ is the mechanical impedance of the PT patch.

For the monitoring of the health of a structure with the EMI technique, it is necessary to quantify variations in the electrical admittance signatures obtained from the monitoring process. For that purpose, different damage metrics or statistical indices have been developed. The root mean square deviation (RMSD) has been usually chosen as statistical metric to detect variations of the impedance signatures in different frequency intervals for concrete structures [12]:

$$RMSD(\%) = \sqrt{\frac{\sum_{i=1}^{n}\left[\mathrm{Re}(Z_0(\omega_i)) - \mathrm{Re}(Z_1(\omega_i))\right]^2}{\sum_{i=1}^{n}\mathrm{Re}(Z_0(\omega_i))^2}} \hat{A} \cdot 100 \tag{3}$$

where $Z_0(\omega_i)$ is the impedance of the PT sensor measured before loading the structure in different frequency intervals, $Z_1(\omega_i)$ is the corresponding value once the structure has been already loaded, at the *ith* frequency point and n is the number of testing frequency points in different frequency intervals. As commented previously, the real part of impedance is more sensitive to the changes in impedance signature; then, RMSD index is usually defined in terms of the conductance (real part of the admittance).

However, changes in the impedance signatures can be due to mechanical damage but also to other phenomena such as operational and environmental variations besides the random uncertainties associated with the experimental readings of the structural response. These variations and uncertainties can arise as unwanted effects in the structural responses, affecting damage-sensitive features and masking changes caused by damage. In this sense, the application of the linear mixed effects models might be evaluated as a method to filter changes

in the damage-sensitive features caused by structural damage from those caused by varying operational and environmental conditions and experimental uncertainties.

3. Linear mixed effects models

LMMs are used in this work as a tool to assess the structural integrity of concrete beams strengthened with NSM-FRP bars. This type of models is an extension of linear regressions models describing the relationship between a responsive variable and independent variables and allow to handle data with repeated measures as those due to the impedances captured in different sensors along different loading stages applied on the beam. In LMMs the data to be analyzed are modelled as the additive combination of fixed effects, random effects and independent random errors. Fixed-effects terms are usually the regression part, i.e. the factors of interest we manage in the study, while the random effects are generally associated with individual experimental units drawn from a population whose specific level values we actually do not care about.

In our particular scenario, we want analyze with a LMM how the RMSD index is affected by the possible variations introduced by the successive loading stages applied on the beam. If variations are due to mechanical damage, RMSD evolution might give us an indication about the real condition of the structure. In this sense, RMSD index would be the responsive variable (or the dependent variable) of the problem, while the condition or damage stage of the beam would be the explanatory variable (or the independent variable). This relationship can be expressed with the following equation:

$$RMSDd\tilde{a}mage\_state \tag{4}$$

The independent variable is also referred to as fixed effect.

However, it cannot be stated that the variations of RMSD index are only completely determined by the damage state. There are other factors such as the frequencies used in the experimental tests, the type of sensors, the experimental conditions or any other elements that might influence the RMSD.

Experimental tests are performed over a defined range of frequencies. We should expect that the RMSD index might also be affected by this range. Different frequency ranges might affect in a different way to RMSD. This effect can be controlled and, therefore, is a fixed effect. With the addition of this effect the previous model becomes

$$RMSDd\tilde{a}mage\_state + frequency \tag{5}$$

However, there's one important point that we have missed. One of the key assumptions of this model is that all measurements must be independent from each other. Since every sensor has been used to compute the impedance several times during the loading procedure, it is to be expected that there will be a certain correlation in the values that it has measured. Therefore, multiple responses from the same sensor cannot be regarded as independent from each other. In our scenario, every sensor, either due to its type or due its location on the beam, has different characteristics that affect to its measurements and, therefore, these must be considered interdependent or correlated rather than independent. To deal with this, the model proposes adding a random effect for the sensors. That way, the model assumes a different baseline for each sensor, and estimates a different baseline for each. This is how this model deals with this issue and resolves the non-independence. That way, the expression to model the RMSD becomes the following

$$RMSDd\tilde{a}mage\_state + frequency + (1|sensor) \tag{6}$$

The term "(1|sensor)" is a way of defining the variable sensor as a random variable, so multiple responses should be expected per sensor.

Finally, there will always be some external factors which have not been taken into consideration and might affect the RMSD. They are independent random errors which include all the random or uncontrollable phenomena affecting RMSD and whose variance cannot be explained by the variables of our model. To capture these effects, the previous expression is updated with an error term

$$RMSDD\tilde{a}mageState + frequency + (1|sensor) + \varepsilon \tag{7}$$

The error term, ε, represents the deviations from the predictions due to random factors which cannot control experimentally.

The model (7) is a mixed effects model. The variables are divided into two groups. In the first group, the systematic (the fixed effects, also known as explanatory variables) and the error term would be included while, in the second group, the random effects, which define the characteristic variation that is due to individual differences in the sensors, are included. The mixture of both fixed and random effects is what gives the name to the mixed model.

Finally, a last update of the model will be done. Apart from studying how each of the variables affects the RMSD, we might want to explore if there is any interaction between them. For example, the fact that some frequencies affect the RMSD index more in some damage states than in others. For that purpose, the model should be updated as follows

$$RMSDd\tilde{a}mage\_state * frequency + (1|sensor) + \varepsilon \tag{8}$$

Equation (8) corresponds to the final expression of the linear mixed effects model which will be used in this work. However, before its application, the model requires to check if some conditions or assumptions are satisfied. These assumptions are usually tested graphically, plotting the model residuals (the difference between the observed values and the model-estimated values) against the predictions.

- Linearity: LMMs are based on the assumption that the data follow a straight line This condition is met when the residuals of the model do not show any obvious pattern when plotted against the fitted or predicted values.
- Absence of collinearity. To meet this condition the predictors used in the model cannot be correlated.
- Homocedasticity. This condition is met when the residuals have a similar amount of deviation from the predicted values regardless of the fitted value, i.e. the variance of the residuals for each fitted value is similar.
- Normality of residuals: LMMs assume that the residuals of the analysis are normally distributed. Q-Q plots (quantile–quantile plots) are useful to give an estimation of where the standardized residuals lie with respect to normal quantiles. If a strong deviation from the provided line occurs, it is a symptom of non-normality of the residuals. In this study, Gaussianity was also tested using Shapiro-Wilk and Kolmogorov-Smirnov tests.

However, the normality of residuals assumption is the one that is least important [17], since these models are robust even to the absence of normality in the data.

Sometimes the normality of the residuals is improved performing a log transformation of the data.

- Independence. The independence is guaranteed when there is no correlation between one measurement and the next one. As we have explained before, we solve the potential non-independency created by the sensors by using a random effect variable.

In this work, the LMM models were estimated using the lme functions of the R library [28]. Although, there is no a single correct way to implement an LMM, residual maximum likelihood has been used here to estimate variance parameters because they are less biased than both maximum likelihood estimates and method-of-moment estimates obtained from residuals of a fitted trend.

4. Experimental tests and validation of the method

Two laboratory tests were carried out on two beams to experimentally validate the proposed method used to detect and distinguish the different damage scenarios.

4.1. Specimen A

4.1.1. Experimental set-up

The first specimen was designed to be tested on the short term. The predicted damage mode for this beam was the rupture of the composite reinforcement at the central section under bending stress. To promote this, an initial crack was induced at the center of the beam. The test carried out was a four-point bending test. The reinforced beam was cast with a length of 1.7 m, a width of 0.12 m and a height of 0.18 m such as shown in Fig. 1. A CFRP strip was inserted on the cover of the beam following the NSM method. The material properties of the concrete, the reinforcement steel and the CFRP were the following: a) Concrete: f_c = 30 MPa, E_c = 26 GPa, f_{ct} = 3 MPa; b) Steel: f_y = 500 MPa, E_s = 210 GPa; c) CFRP: f_{fu} = 2500 MPa, E_f = 170 GPa.

Additionally, the characteristics of the strenghtened section were theoretically calculated prior to the test assuming that the rupture mode is via the breakage of the FRP strip (Fig. 2). The computed characteristics were the following: M_{cr} = 1.94 kNm, M_y = 5.04 kNm, M_u = 9.79 kNm, P_{cr} = 6.5 kNm, P_y = 16.8 kNm, P_u = 32.6 kNm.

Concerning the instrumentation of the beam, eight PZT sensors were bonded in different locations such as shown in Fig. 3. The PZT sensors measured the electromechanical impedance after each loading state, once the beam was in a resting state. Moreover, sensors PZT1 and PZT2 were of different size from sensors PZT3 to PZT9 in order to investigate the sensitivity of different types of sensors. Additionally, sensors PZT6 to PZT9 were embedded inside the concrete beam and attached to the FRP to examine the difference in damage detection capability between these sensors and the sensors PZT3 and PZT4, which were surface-bonded. For purpose of illustration, sensors PZT2 and PZT4 are shown in Fig. 4 once the beam has reached its ultimate limit state.

Concerning the loading procedure, 6 loading steps were applied on the beam until its rupture which was reached at step 6. For each loading step, the beam was subjected to three cycles of loading and unloading, reaching the charge defined for each step at the end of every loading. The purpose of this method was to stabilize the cracks that appeared on the beam after each loading step. The programmed loads reached at each loading step for specimen A are indicated with red points in the load–displacement plot shown in Fig. 2. Additionally, the real evolution that these loading steps followed during the experiment is shown in Fig. 5 for a strain sensor bonded to the FRP bar and located where the left load point applies. The correlation with the initially proposed loading steps is clearly observable. First cracks appeared during the second loading stage and grew during the subsequent loading stages. Additionally, yielding initiated during the fourth loading stage.

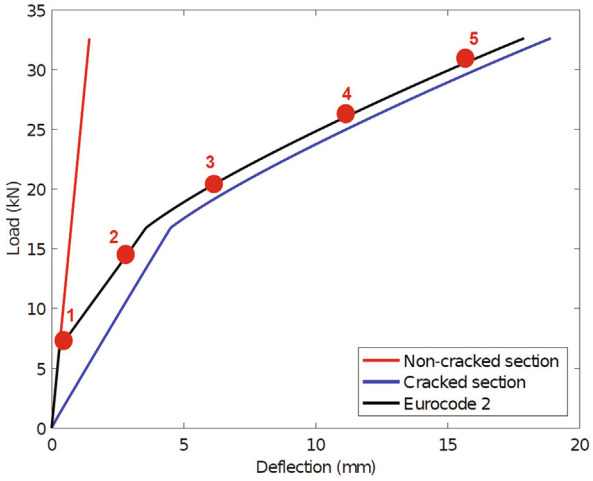

Fig. 2. Load-Displacement curve for the tested beams.

As commented previously, the electromechanical impedances were measured initially and after each loading step. The initial measurement, defined as the impedance signal at the healthy state (damage state 0), served as a baseline for comparison. Five frequency sweeps of 1 V were conducted for each sensor at each damage state, resulting in 5 impedance signals that were averaged in order to obtain the impedance signal that would be later on used for the damage assessment. These sweeps covered the frequencies from 10 kHz to 100 kHz with a frequency step of 12.5 Hz. Thus, seven measurements were taken for each PZT sensor for this experiment, although the signals after step 6 were not very useful because the beam was already in a severely damaged state. When a damage state is referred to for a PZT sensor, that damage state is considered to be the measurement taken after that same load step (i.e. damage state 3 refers to the measurements taken just after the loading step 3). Only very small variations of temperature occurred during the tests since they were carried in a short period of time under controlled laboratory conditions, therefore, no temperature compensation was needed.

Fig. 6 shows the real part of the impedance spectrum captured by sensors PZT1 and PZT6 for the baseline and the five loading stages. Considering the insufficient energy in actuating signal, a PZT only monitors a limited area around itself and the EM signature contains the local dynamic information of the structure. Except when the damage is already severe, from the observation of Fig. 6 it is difficult to get to get some information about the evolution of damage which demonstrates the importance of applying a suitable analysis tool for it.

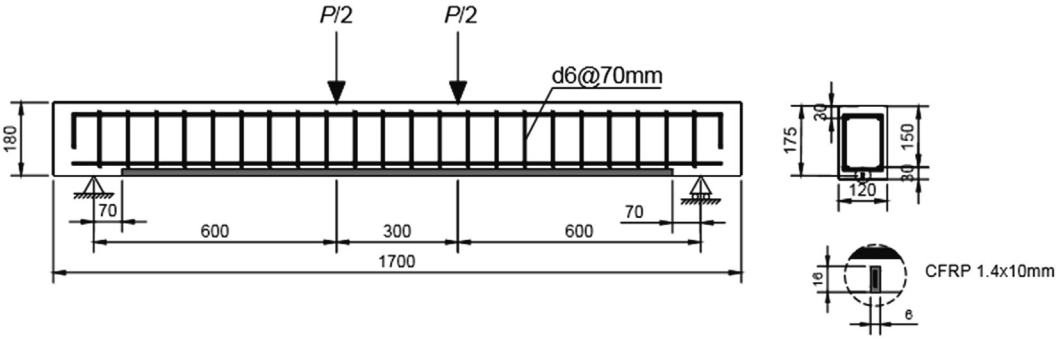

Fig. 1. Geometry and loading scheme – Experimental beams.

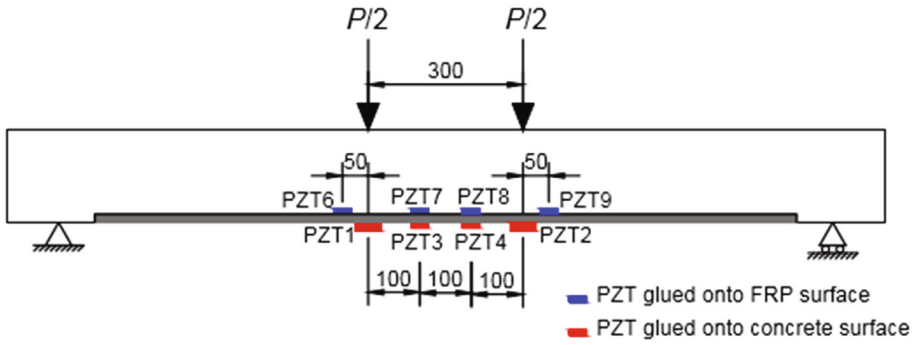

Fig. 3. Experimental layout for the PZT sensors – Specimen A.

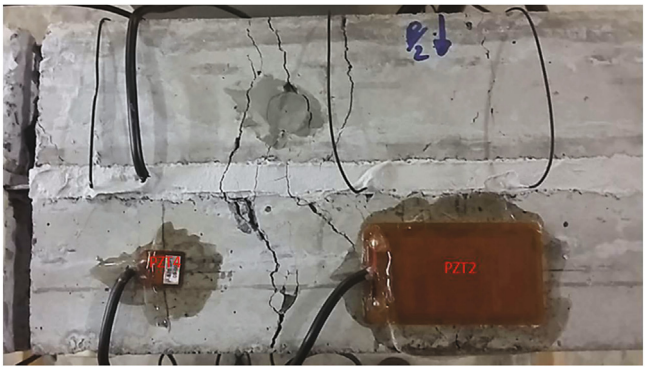

Fig. 4. PZT sensors 2 and 4 on the beam after the damage state 6.

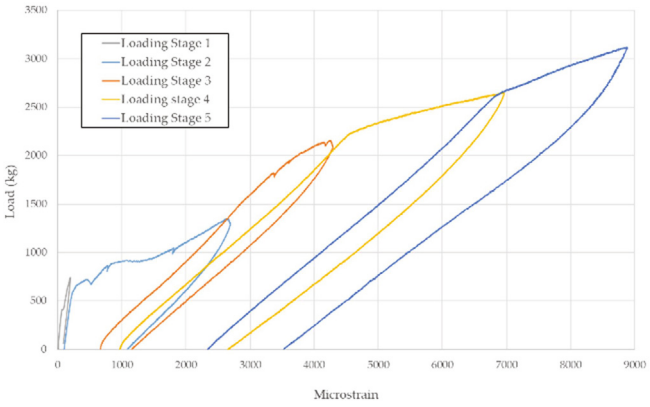

Fig. 5. Experimental load vs microstrain – Specimen A.

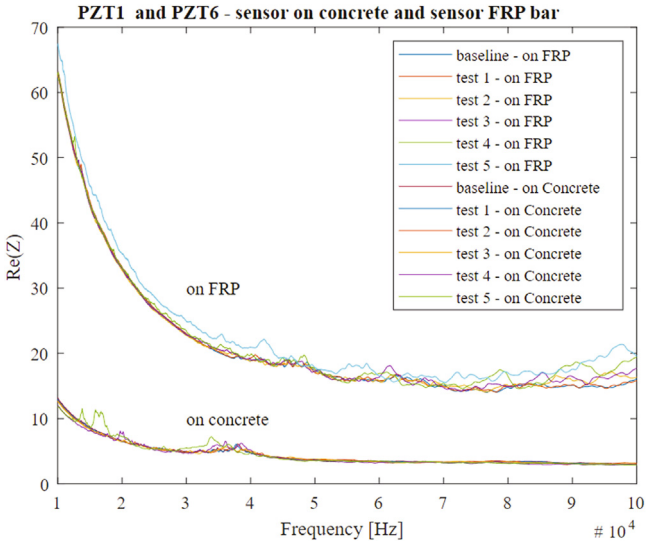

Fig. 6. Impedance spectra of the real part of the impedance.

4.1.2. Slope-based RMSD index

A study was firstly performed from the computed RMSD values for all the sensors and loading stages taking as baseline for their calculation the impedance signal associated to the undamaged state (state 0). This initial study will be useful to get in a simple way a first view about the changes experienced by the specimen in different areas along the loading procedure. A slope-based RMSD index [29] will help us to understand better how the evolution of the RMSD index is affected by the severity of the changes.

Fig. 7 shows the RMSD values for all sensors and loading stages together with the fitted straight line characteristic of the slope. RMSD values for state 0 have been included by comparing the five frequency sweeps that were done by each sensor at initial state.

As expected, RMSD values show a tendency to increase as the applied load increases. This tendency is shown in all sensors, so it provides useful information to assess the structural integrity of the beam. In addition, it can be observed how the RMSD indices for states 4 and 5 are significantly higher than for the rest of loading states for all sensors, and, therefore, all sensors report the same consistent information regarding the possible severity of changes at the last steps. This effect is clearly noticeable in sensor PZT2, where RMSD indices show a drastic increase after step 4. In summary, two important conclusions can be extracted from this figure. First, all sensors show a clear distinction between initial state and the rest of loading states, which means that all sensors were able to detect the progressive changes experienced by the beam. Second, since the RMSD increases as the changes propagate, all sensors are capable to capture the increasing severity of these changes.

The second result pertains to the slope of the RMSD values. The fact that the slope for PZT2 is the greatest correlates with the fact that more severe changes occurred in the vicinity of this sensor during the last loading steps. In addition, the slope for this sensor is much greater than for PZT1. Also, the fact that both sensors, PZT3 and PZT4, show very similar slopes is remarkable and indicates that both sensors have very similar behaviors.

All sensors but sensor PZT8, show an increasing RMSD index with the loadsteps. However, as it was explained before, the potential of the slope-based RMSD relies on the fact that single outlying values do not drastically change the conclusions, as the sensor PZT8 has a positive slope. Therefore, although this sensor has not given the most important information of all sensors, it still shows and increasing trend in the RMSD indices, meaning that it has also been able to detect the pos-

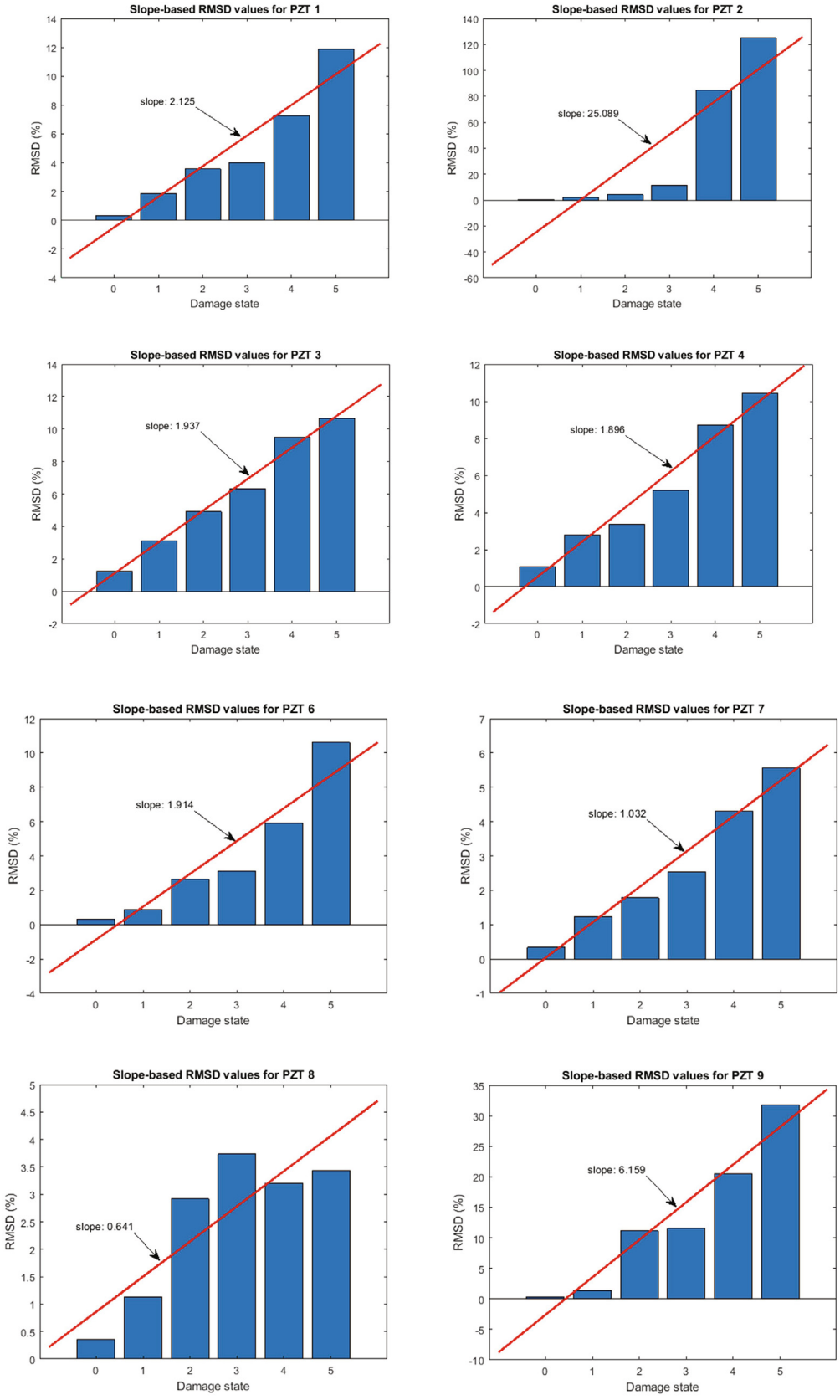

Fig. 7. Slope-based RMSD values – Specimen A.

sible growth of the changes. Concerning the rest of sensors, we can appreciate the same behavior as with the previous sensors. They all show higher RMSD values for higher loading states, and damage states 4 and 5 stand out from the rest of states. In addition, the RMSD and the slope-based RMSD show the most severe variation for PZT9 in comparison with the rest of internal sensors.

4.1.3. Application of LMMs

In the previous section, we have checked that RMSD index experiences some changes along the different loading states which might be interpreted as growing damage. However, before stating clear conclusions there is an important issue which has not been fully addressed yet: How likely is that the variation in the RMSD index is due to the loss of structural integrity of the beam? There are various factors which might affect to this metric such as the type of sensor, the excitation frequency used or the damage state. Therefore, firstly, to set some conclusions about the performance of the beam, we should assess how responsible each of these factors is in the variation of the RMSD index.

Secondly, if it is proved that the damage state has a significant influence on the RMSD index, we should study how different each of the individual damage states are from each other. The main objective is to tell apart the damage states amongst themselves. Additionally, a deeper study will be performed too in this section examining the influence of the type of sensor and the frequency of excitation on the damage detection performance.

In order to achieve the first purpose, we will use a linear mixed effects model such as presented in Section 3. As explained previously (Eq. (8)), the fixed variables for the model will be the damage state and the frequency interval, while the random variable will be the type of sensor. We will be working with 5 possible damage states (1 to 5), 9 frequency intervals (intervals of 10 kHz, from 10 kHz up to 100 kHz) and 8 sensors (PZT1 to PZT9). In this way, each data point in this analysis corresponds to the RMSD value for a specific sensor, at a certain damage state, calculated in a specific frequency interval, leading to a total of 360 data points. The first objective of the analysis will be to study if the damage state and/or the different frequency ranges have a significant influence on the RMSD. If so, a post-hoc analysis will be performed to study if there are significant differences amongst the different levels within each fixed variable. In other words, if it is demonstrated that the damage state has a significant influence on the RMSD, then it's justified to perform a pairwise comparison to study if there are differences between each pair of damage states. This would help us understand if the sensors are able to recognize the growing damage in the beam.

The first analysis will be focused on studying the potential influence of the damage state on the RMSD using initially all the sensors as a whole and using subsequently separately three different groups of sensors. Group 1 includes sensors PZT1 and PZT2, which are the larger surface-bonded sensors. Group 2 includes sensors PZT3 and PZT4, which correspond to the smaller surface-bonded sensors, and group 3 includes sensors PZT6, PZT7, PZT8 and PZT9, which are all embedded sensors of the same type. The objective of performing this analysis split in three groups is to study how the type and condition of a sensor affects to the damage sensitivity. Finally, another analysis will be performed focused on the frequencies, in order to understand which frequencies, if any, have more influence on the RMSD or help differentiate between damage states better.

Before heading directly to the statistic results, it is needed to examine firstly if the model conditions, sketched out in Section 3, are met. The procedure to be followed will be shown here for all sensors jointly but it will be similar when working with each one of the three groups of sensors.

As a first step, it is interesting to examine the data and test if they follow a normal distribution for each loading state required to carry out an analysis with LMMs. Although what we really need to test are the residuals of the model, it is always a good idea to first have a look at the raw data. The RMSD index histograms for each loading state and considering all sensors are shown in Fig. 8. Histograms provide a visual judgment about whether the distribution is bell shaped. As it can be observed, these data do not appear to follow a normal distribution. In order to further prove this hypothesis, Shapiro-Wilk method is widely used for normality tests. When this test is applied on some experimental data, it tells us if the data have a significant departure from normality by comparing the sample distribution to a normal one. For it, the main parameter to inspect in this test is the p-value. The p-value can be seen as the probability of our data following a normal distribution given our dataset. Low p-values (typically below 0.05) mean that there is a significant departure from normal distribution in the data while values above the threshold imply that the distribution of the data is not significantly different from normal distribution. Table 1 shows the p-values derived from the Shapiro-Wilk test. It is clear that there is a significant departure from normality for all loading states (i.e. all tests provide a p-value lower than 0.05). However, as it was previously commented, it is important to test the normality of residuals, although this first analysis makes us think that the residuals will not follow a normal distribution either. Residuals are estimated using the model shown in Eq. (8).

Figs. 9 and 10 show the Q-Q plot and the histogram of the residuals, respectively. These two approaches allow to check initially the normality by visual inspection. Q-Q plots draw the correlation between a given sample and the normal distribution. For the residuals to follow a normal distribution, the data points in the Q-Q plot should adjust to a straight line. From the figures, it cannot be stated that the residuals of the model follow a normal distribution. To further support this hypothesis, a significance test is applied on the residuals using the Shapiro-Wilk method. A p-value of 2.2e-16 is obtained, which confirms a significant departure from normality. To solve this issue, we should apply some kind of transformation on the data in order to obtain more reliable results.

In addition to the normality assumption, it is also important to test the linearity and homocedasticity assumptions such as commented in Section 3. This can be done by plotting the fitted values against the residuals of the model (Fig. 11). As it can be observed, Fig. 11 shows obvious heteroscedasticity (the opposite of homocedasticity). Higher fitted values lead to higher absolute residuals, i.e. the variability of the residuals is unequal along the range of fitted values. This means that whenever the model is being less accurate the higher the fitted values are, and therefore the variance is higher in the higher range, which is not what we are looking for in the model. Therefore, the homocedasticity condition is not met. In addition, it would not be accurate to assume that the residuals do not show any obvious pattern, and therefore it cannot be stated that the linearity condition is met.

There are several possible solutions to address the issue of heteroscedasticity and non-normal distribution of residuals. One of the most widely used is using a non-linear transformation of the response, such as the log-transform. In order to test if the data follow a log-normal distribution, it is possible to use the Kolmogorov-Smirnov test. Similar to the Shapiro-Wilk test, the Kolmogorov-Smirnov test tells us if the data has a significant departure from log-normality. In this case, the p-value can be seen as the probability of our data following a log-normal distribution given our dataset. As in the case of the Shapiro-Wilk test, low p-values (typically below 0.05) mean that our data show a significant departure from log-normality. Table 2 shows p-values computed from the Kolmogorov-Smirnov test for each loading stage considering all the sensors. None of the loading stages shows a significant departure from log-normality (i.e. all p-values are above 0.05), from which we can infer that the data might follow a log-normal distribution. It justifies to create a new variable, logRMSD, computed from the log-transform of the RMSD indices. The model becomes now the following

$$log(RMSD)\tilde{damage\_state} * frequency + (1|sensor) + \varepsilon \quad (9)$$

Figs. 12 and 13 show the Q-Q plot and the histogram of the residuals, respectively, according to the new model based on the log-transform. Both figures show that the residuals now follow a distribution much closer to a normal. The data points in the Q-Q plot adjust well to the straight line up to the last few data points, and the his-

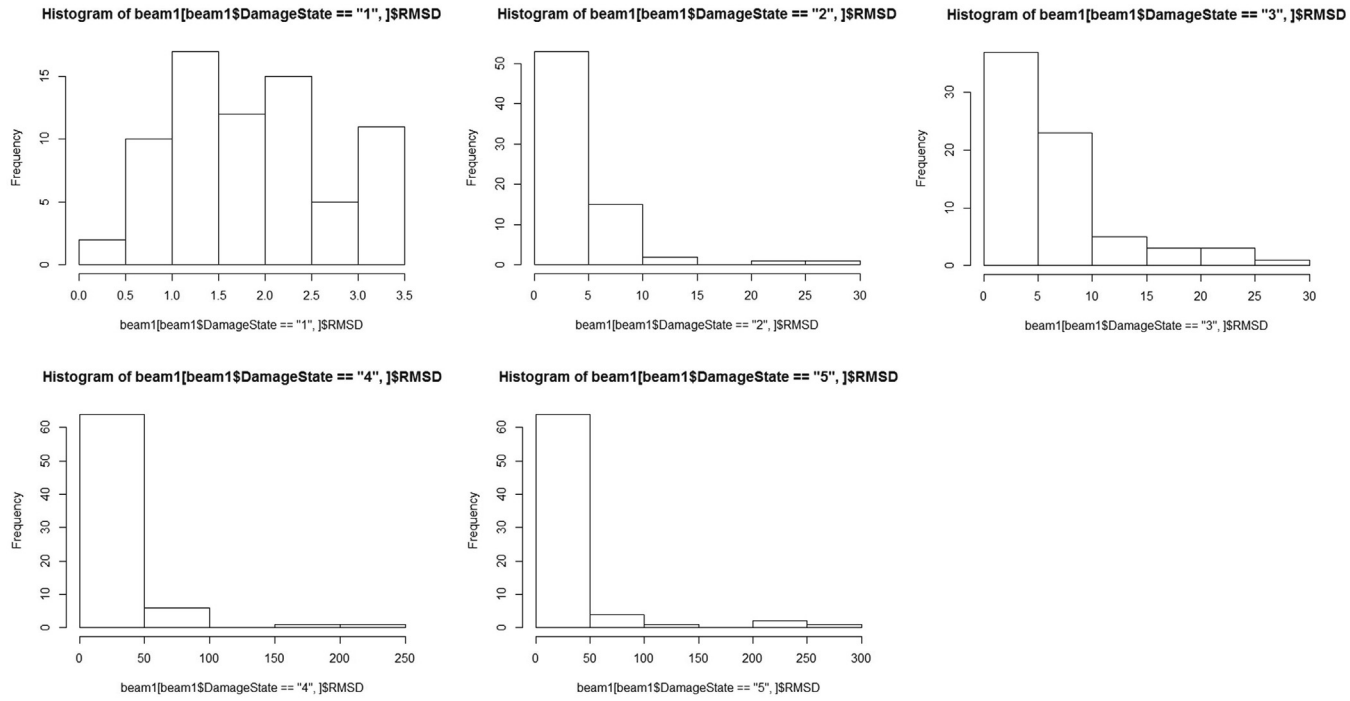

Fig. 8. RMSD histograms for each damage state- Specimen A.

Table 1
Shapiro-Wilk normality test – Specimen A.

	Loading stage 1	Loading stage 2	Loading stage 3	Loading stage 4	Loading stage 5
p-value	0.01404	4.785e−11	1.168e−8	3.573e−15	5.052e−15

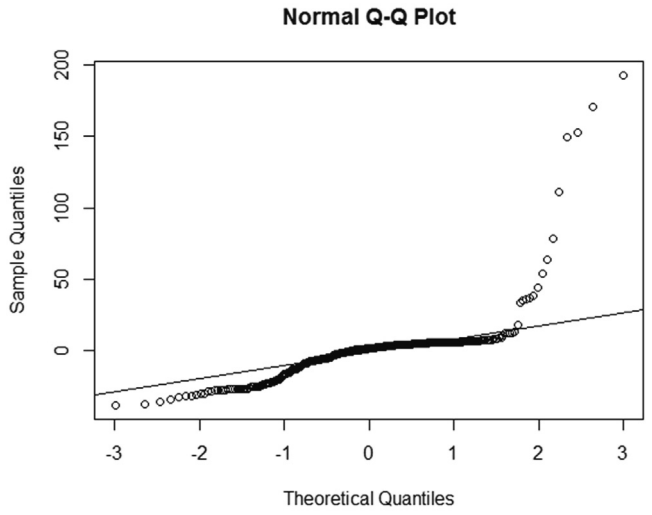

Fig. 9. Q-Q plot for the normality test – Specimen A.

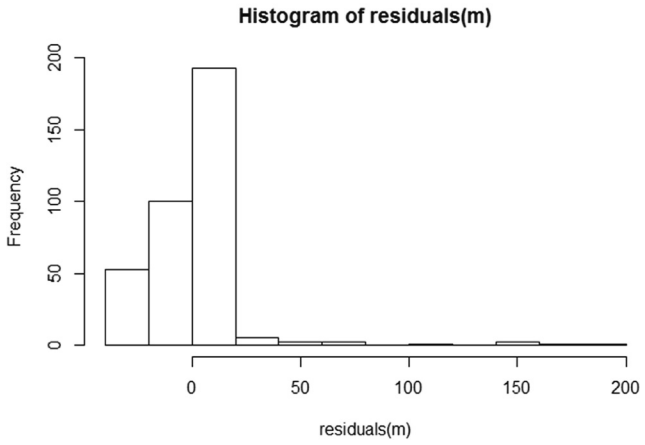

Fig. 10. Histogram of the residuals including all the dataset – Specimen A.

togram of the residuals has a shape that adjusts better to the typical bell curve. Therefore, it can be assumed that the dataset will give more reliable results, as it complies better with the normality assumption.

After this, we proceed to test the linearity and homocedasticity assumptions for the model of Equation (9). This can be done, as previously, by plotting the fitted values against the residuals of the model (Fig. 14). As it can be observed, the variance of the residuals is not dependent on the fitted value, so we can conclude that the homocedasticity condition is not violated. In addition, there is not any obvious pattern in the residuals, and therefore the linearity assumption is also met.

Finally, up to this moment three out of the five conditions listed previously have been met by the model. Concerning the absence of collinearity condition, this is met by considering the fact that the two fixed variables of the model (damage state and frequency) do not have any apparent relationship. The damage state is not defined by the frequencies used; in fact, damage states 1 to 5 would have the same progression regardless of the frequencies at which the sensors operated. Therefore, it can be stated that there is no collinearity in the

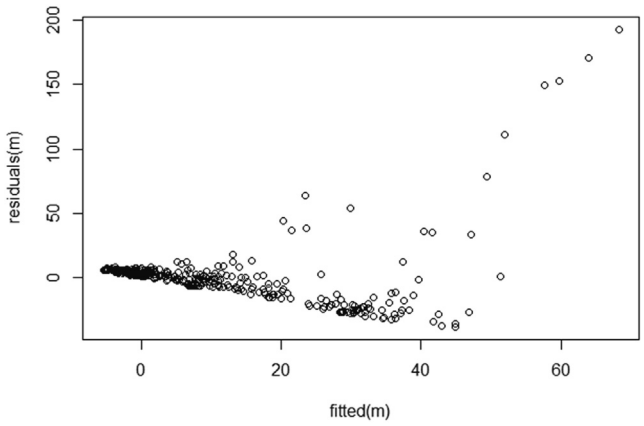

Fig. 11. Fitted vs residual values for the model – Specimen A.

data. On the other hand, regarding the independence condition, it has been explained previously that this assumption is met by the introduction of the random effect on the model, thus removing the potential non-independencies that the sensors could introduce.

Once we have checked that the conditions required by the model are verified, it is justified to perform an analysis on the data. As explained before, the first objective will be to prove that the damage variable has a significant influence on the RMSD value. If so, we will proceed performing a post-hoc analysis doing pairwise comparisons in order to assess if there is a significant difference between each pair of damage states.

To reach the first objective, an analysis of variance (ANOVA) using a F-test will be performed for model objects produced by LMM. This analysis will give us a p-value which can be interpreted as follows. The null hypothesis in this model is that the damage state and the frequency do not have effect on the RMSD. A low probability or p-value indicates that the sample data are unlikely when the null hypothesis is true. According to this, the p-value is a conditional probability, it is a probability under the condition that the null hypothesis is true. Therefore, if we have a very low p-value, we can reject the null hypothesis and, therefore, the damage state and the frequency affect to RMSD value. We can rephrase the p-value in this way: what is the probability of observing our particular set of RMSD data if the damage state (or the frequency) has no effect on the RMSD?

Table 3 shows the p-values computed from the analysis of deviance for the LMM. There are three important conclusions that can be extracted from this analysis. First, it proves that the damage state has a significant influence on the RMSD, since the p-value for this variable is significantly smaller than 0.05. This is an important conclusion since it has led us to prove that, amongst all variables, the damage state influences the RMSD significantly, and therefore it is reasonable to use this damage metric to assess the structural condition of the beam. In the same way, this analysis also proves that the frequency interval has a significant influence on the RMSD, i.e. RMSD index will be sensitive to the frequency range. Finally, from this analysis we can also conclude that there is no significant interaction between the damage state and the frequency.

This overall analysis allows us to perform a second analysis where we test how different each damage state is from the rest. Fig. 15 shows the boxplots for each damage state. As it can be observed, there is a variation in the log(RMSD) value when we move from one damage state to another. What the pairwise comparisons will do is evaluate if this change is significant enough to affirm that the sensors have captured the increasing damage in the beam (Table 4). As in previous analyzes, what we need to inspect here is the p-value. A p-value smaller than 0.05 means that there is a significant difference between that pair of damage states, and therefore the model has successfully distinguished them. This analysis yields an important result, which is that the sensors have been able to distinguish between every pair of damage states with a significant confidence. Damage states 2–3 and 4–5 are the pairs for which the significance level is the lowest (i.e. the p-value is the highest), and still for these pairs the p-value is below the limit of 0.05. As a conclusion, it can be asserted that this method has been able to distinguish amongst all damage scenarios with a significant confidence.

Once an overall analysis has been carried out, the same analysis will be performed but this time focusing on each group of sensors. For it, the same procedure as in the previous analysis will be followed. Although not shown here for simplicity, the model assumptions are not satisfied for any of the groups when working directly with RMSD and, because of it, a new variable consisting of the log(RMSD) value is defined for each group. At this point the model assumptions will be checked again considering the model with the new variable. If this test gives enough confidence to continue with the analysis, the analysis of variance test will be performed. Finally, if this test shows that the damage state and/or the frequency have a significant influence on the RMSD index, post-hoc analysis with pairwise comparisons will be carried out.

To avoid repetition, the whole test of assumptions will not be presented since it was made for the previous analysis. Instead, the Q-Q plot (Fig. 16), the histogram of the residuals (Fig. 17) and the fitted vs residual values plot (Fig. 18) will be displayed in order to prove that the assumptions have been met. For all groups, the data points in the Q-Q plot adjust well to a straight line and the histogram of the residuals resembles the typical bell curve. Therefore, it can be guessed that the residuals will meet the normality assumption. Moreover, according to Fig. 19, it can be observed that there is not any obvious pattern in the residuals, so it can be concluded that the linearity assumption is not violated. In addition, from the scatter of the data points it can be assumed that the variance of the residuals does not have a clear dependence on the fitted value. For this reason, the analysis will be continued considering that the homocedasticity assumption is not violated.

After the model assumptions have been tested, the analysis of the data will be performed. As explained previously, the first objective will be to prove that the damage state variable has a significant influence on the RMSD index. If so, a post-hoc analysis will be made to perform pairwise comparisons in order to assess if there is a significant difference between each pair of loading stages. Results from the first analysis of variance for the three groups of sensors are shown in Table 5.

Following the same logic as we did for the overall analysis, the study will be focused on the p-value for each variable. As it can be observed, the p-value is much lower than 0.05 for the damage state variable, meaning that the damage state has a significant influence on the RMSD. Therefore, the three groups of sensors are able to capture the presence of the damage, as this variable affected significantly the RMSD index. On the other hand, neither the frequency nor the interaction of the frequency with the damage state have shown a significant influence on the RMSD for groups 1 and 2. For this reason, a further post-hoc analysis for the frequency variable is not justified.

Table 2
Kolmogorov-Smirnov test – Specimen A.

	Loading stage 1	Loading stage 2	Loading stage 3	Loading stage 4	Loading stage 5
p-value	0.5074	0.4991	0.7454	0.08232	0.1358

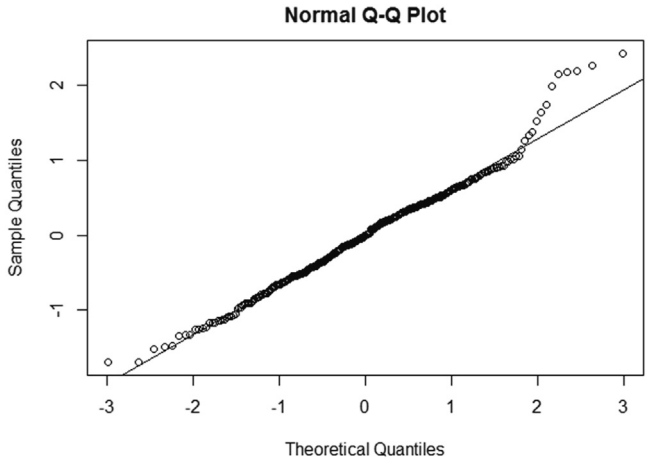

Fig. 12. Q-Q plot for the normality test using log (RMSD) – Specimen A.

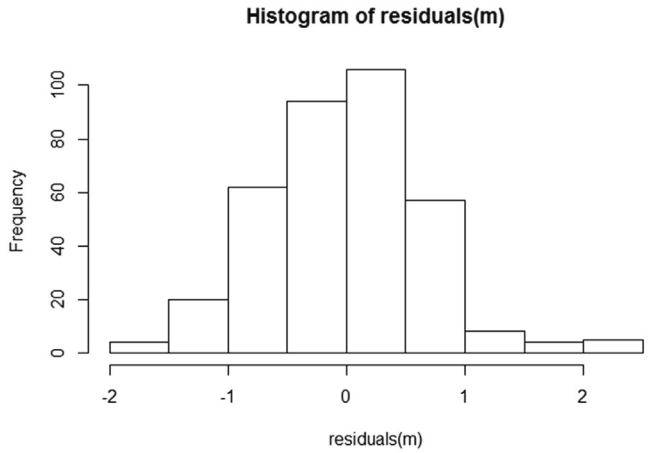

Fig. 13. Histogram of the residuals using log (RMSD) – Specimen A.

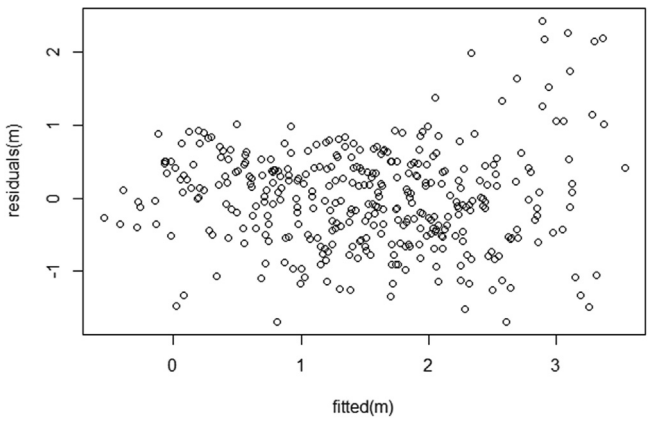

Fig. 14. Fitted vs residual values for the model using log(RMSD) – Specimen A.

Table 3
Analysis of deviance – Specimen A.

	Damage state	Frequency	Damage state:frequency
p-value	2.2e−16	4.375e−8	0.9808334

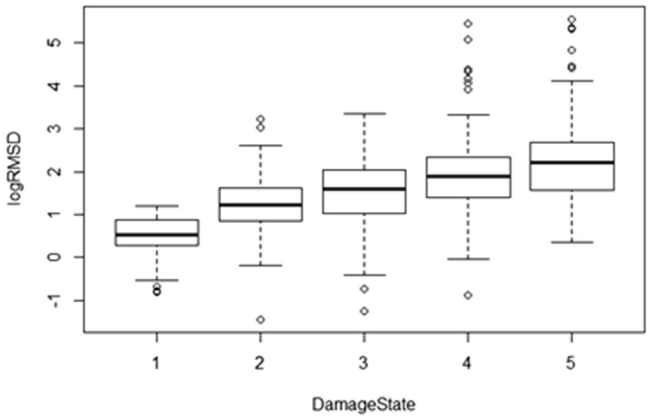

Fig. 15. Boxplots for each damage state – Specimen A.

Table 4
Damage states pairwise comparison – Specimen A.

Damage states	p-value
1–2	3.09e−8
1–3	6.22e−15
1–4	<2e−16
1–5	<2e−16
2–3	0.018530
2–4	4.04e−9
2–5	<2e−16
3–4	0.000532
3–5	3.19e−9
4–5	0.018530

However, for group 3, the frequency variable has a significant influence on the RMSD, yielding similar results to the overall analysis; this means that sensors of group 3 play a more important role in the damage detection than the other two groups.

In a second analysis, the difference between the different loading stages (and damage stages) is tested. Boxplots shown in Fig. 19 confirm that there is an appreciable change between some pairs of damage stages, but the high variance of the data is such that for some cases it is not clear that all damage stages are different from each other. A pairwise analysis will help to understand better which pairs of damage stages are significantly different from each other (Table 6).

From Table 6, as it can be noticed, this first group of sensors fails to detect a significant difference between almost every pair of two consecutive damage states (1–2, 2–3, 3–4, 4–5) which means that damage increment between two consecutive damage stages is small for sensors belonging to this group. However, these sensors are able to detect a significant difference for the rest of pairwise comparisons, meaning that they capture the growing damage in the beam.

As a conclusion, it can be stated that Group 1 of sensors has been useful to detect the presence and propagation of the damage. However, they only managed to do so when the damage states were more separate to each other than in the overall analysis, since they had a weak performance at differentiating consecutive damage states. Something similar occurs for Group 2. They are able to distinguish between the most severe damage scenarios (4 and 5) and the initial ones (1 and 2) but they fail to distinguish between damage states that are closer to each other, and, therefore, significant growth of damage between consecutive loading stages is not evident. The analysis of Group 3 yields the most relevant results. As it can be observed, sensors of Group 3 are able to distinguish between almost every pair of damage states. Only for pairs 2–3 and 3–4 the p-value is higher than 0.05, and even for pair 3–4 the p-value is lower than 0.1, still partially significant. As a conclusion, it can be stated that the sensors PZT6, PZT7, PZT8

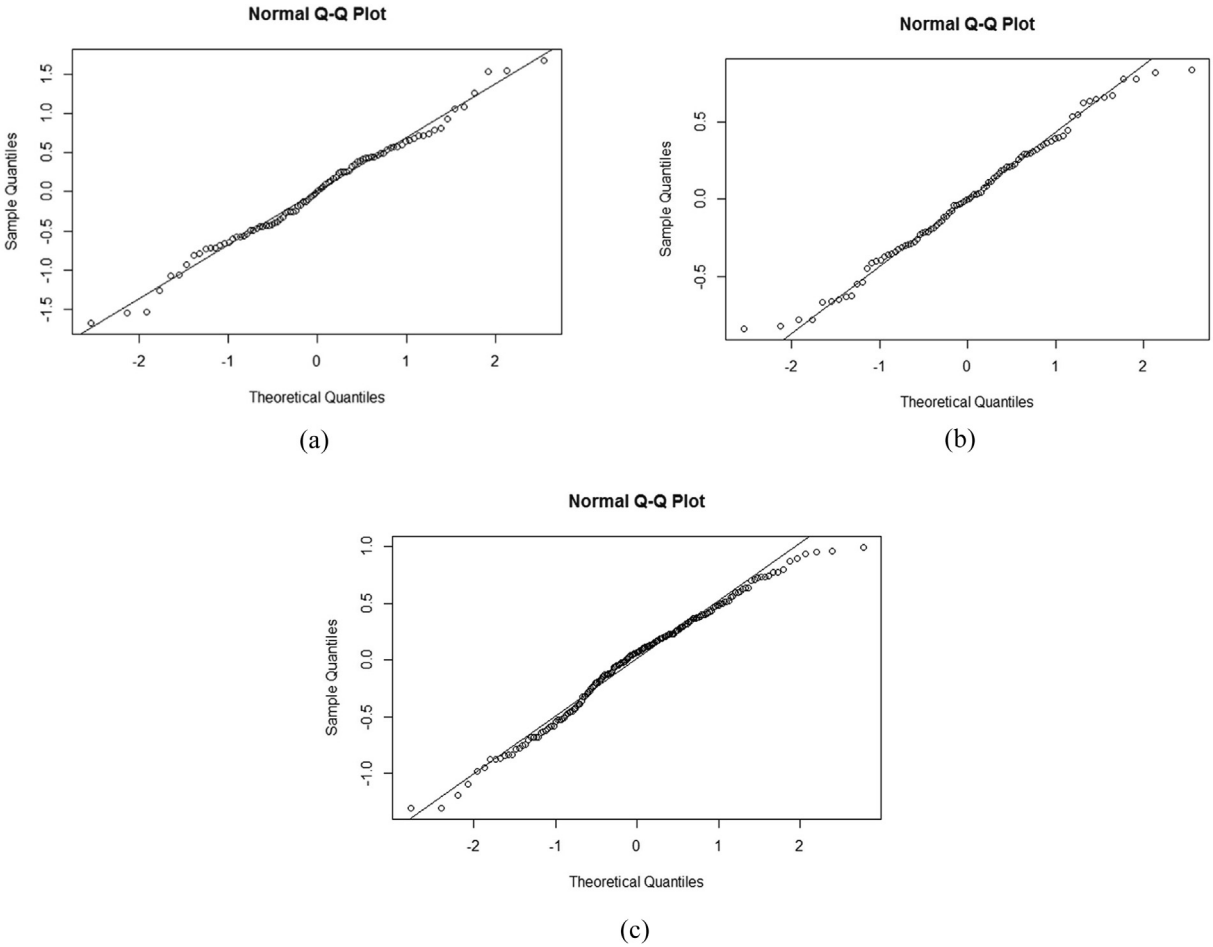

Fig. 16. Q-Q plot for groups (a) 1, (b) 2 and (c) 3 – Specimen A.

and PZT9 have shown the best performance amongst all groups at detecting the presence and propagation of the damage which is a symptom that failure of the beam originated internally where sensors of group 3 were bonded.

A further study was performed focused separately on sensors of group 3. Table 7 shows the p-values for the damage state obtained from an analysis of variance carried out for model objects produced by LMM. As expected, damage state has a significant influence on the RMSD of each internal sensor, especially for PZT6 and PZT9.

Fig. 20 shows the evolution of the boxplots for each internal sensor along the different loading stages. Due to the high variance of the data, apparently, only for sensors PZT6 and PZT9 the identification of the growth of damage is clear. A pairwise analysis will be useful to analyze this in more detail (Table 8). The most critical sensors are PZT6 and PZT9. Results about these sensors demonstrate that an anomaly occurs in the vicinity of these sensors which might be interpreted as a symptom of a possible imminent failure.

Finally, once the analysis by damage state has been performed, it is also interesting to carry out a second analysis this time focused on the sub-frequency intervals. As shown in Table 5, the frequency variable has a significant influence on the RMSD value when working with sensors belonging to Group 3 (embedded sensors). For this reason, it is justified to perform a post-hoc analysis for this group of sensors with pairwise comparisons amongst sub-frequencies intervals instead of amongst damage states. The objective of this analysis is to study the different sensitivity of RMSD index to different sub-frequency intervals [30] and, if so, how these intervals affect the damage state.

Table 9 shows the results of this comparison for the frequency variable. The numbers on the first column represent the frequency intervals subjected to the comparison. So, number 1 corresponds to frequency interval 10–20 kHz, number 2 corresponds to frequency interval 20–30 kHz and so on, until reaching the 9th interval between 90 and 100 kHz. As it can be observed, the model is able to distinguish clearly between the frequency interval 10–30 kHz and the frequency interval 60–100 kHz, although other intervals (30–40 kHz, 40–50 kHz and 50–60 kHz) show also a significant difference with the highest frequency intervals (70–100 kHz). The conclusion that can be extracted from this analysis is that lower and higher frequencies had significantly different influence on the RMSD index, and therefore the damage states might affect to the sensors differently depending on the excitation frequency.

Once this frequency analysis has been carried out, we want to know if a certain range of frequencies works better at differentiating some damage states over others. Based on the results of Table 9, we will establish two different groups of sub-frequency intervals and perform an analysis considering only the frequencies included in each group. The first group will include sub-frequency intervals 1 to 5 while the second group will include sub-frequency intervals 6 to 9.

Table 10 shows results from the analysis of variance performed on sensors of group 3 considering the two intervals. A significant p-value for the damage state variable is computed for both cases, which allows us to perform a pairwise analysis for the same two sub-frequency intervals. In this pairwise analysis we will study how the different set of sub-frequency intervals are able to differentiate amongst the damage states (Table 11).

As it can be observed in Table 11, the fact of eliminating sub-frequency intervals 1 to 5 led to worse results compared to the analysis performed for Group 3 using all the frequency range (Table 6). While

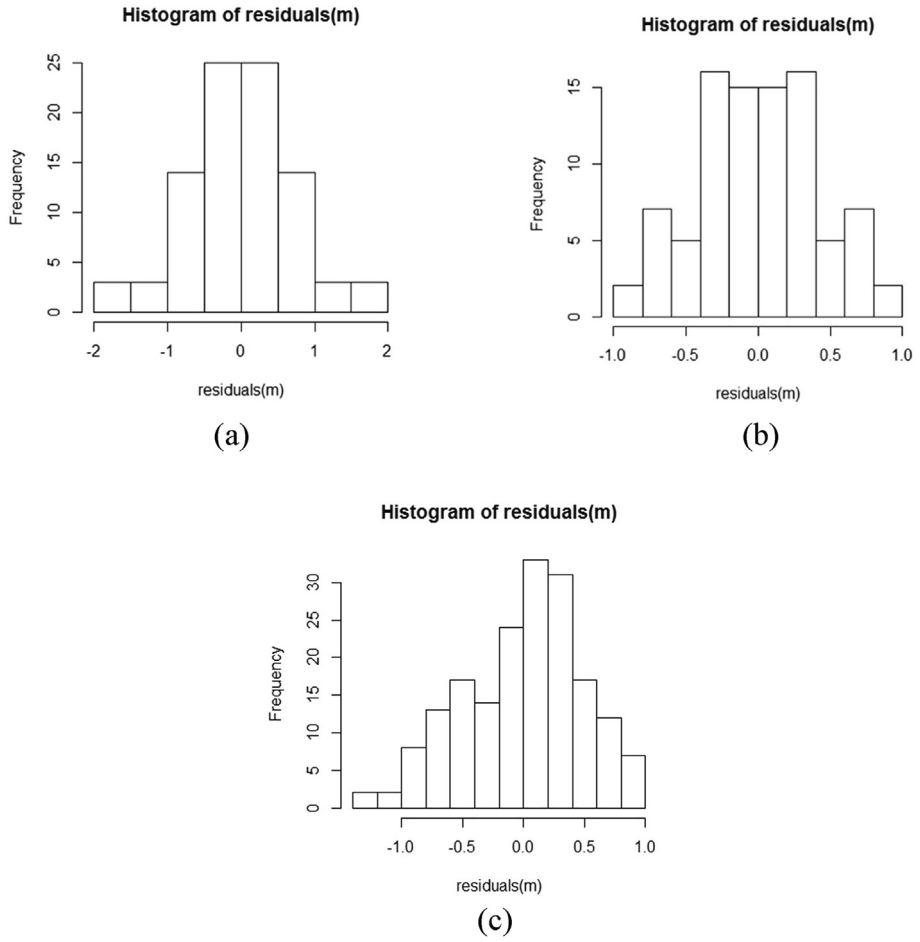

Fig. 17. Histogram of the residuals for groups (a) 1, (b) 2 and (c) 3 – Specimen A.

the analysis for Group 3 showed a significant difference between damage states 4 and 5, this differentiation is lost when we only use sub-frequency intervals 6 to 9. In addition, it does not provide any additional information compared to the analysis of Group 3, since all the damage scenarios distinguished by these frequencies were also distinguished by the analysis of Group 3 with the same significance level. The only difference could be identified in the comparison of damage states 3 and 4, where the model that employs the higher frequencies yields a higher significance level.

On the other hand, if we study the results for sub-frequency intervals 1 to 5, it is interesting to note how the significance level for damage states 4 and 5 is higher than for the analysis of Group 3. This can be due to the fact that the sensors were influenced by the propagation of the damage across the beam rather than in their vicinity, and hence affecting the lower sub-frequency intervals more significantly. Despite this, these sub-frequency intervals were unable to differentiate between damage states 2 and 4 and lost sensitivity in the differentiation of damage states 3 and 4.

As a conclusion, excluding the lower sub-frequency intervals from the dataset led to worse results, as some of the damage differentiation from the Group 3 analysis was lost. Furthermore, excluding the higher sub-frequency intervals led to better results when comparing the last damage states, although the model lost sensitivity when comparing damage states 2–4 and 3–4. Overall, the analysis shows that the best results are obtained when we use a dataset with all the frequency range (10–100 kHz), as the model was able to differentiate amongst the majority of pairs of damage states.

4.2. Specimen B

4.2.1. Experimental set-up

A new test campaign was carried out on a new beam, specimen B, with the same geometric and material properties than specimen A (Fig. 1). However, in this case, the expected damage mode was the delamination of the internal composite reinforcement due to a loss of adherence. To favour this, various areas of the FRP on the left side of the specimen were not attached with epoxy to the concrete in order to induce an initial debonded area at the FRP-concrete interface. Despite this, in the test, the damage mode of the beam was not the predicted one, as the FRP showed a strong adherence and the beam failed by FRP bar rupture. Fig. 21 shows the experimental set-up. Only the portion of the beam between the left support and the applied load is shown since it was the only instrumented region. The same type of PZT sensors than in specimen A was used here, P-876.A12 (PZT1 and PZT2) and P-876.SP1 (the remaining sensors) transducers. The regions shaded in blue in the figure are those which were not bonded initially with epoxy.

An analogous loading and measurement procedure to the one followed with specimen A was carried out on specimen B. Fig. 22 shows the loading–unloading curves for each loading step obtained from a strain sensor located close to the debonded area between sensors PZT8 and PZT9. From the initial baseline stage, six loading steps were applied reaching the failure in the sixth step. The first cracks are not identified in the figure since the strain sensor is located far from the

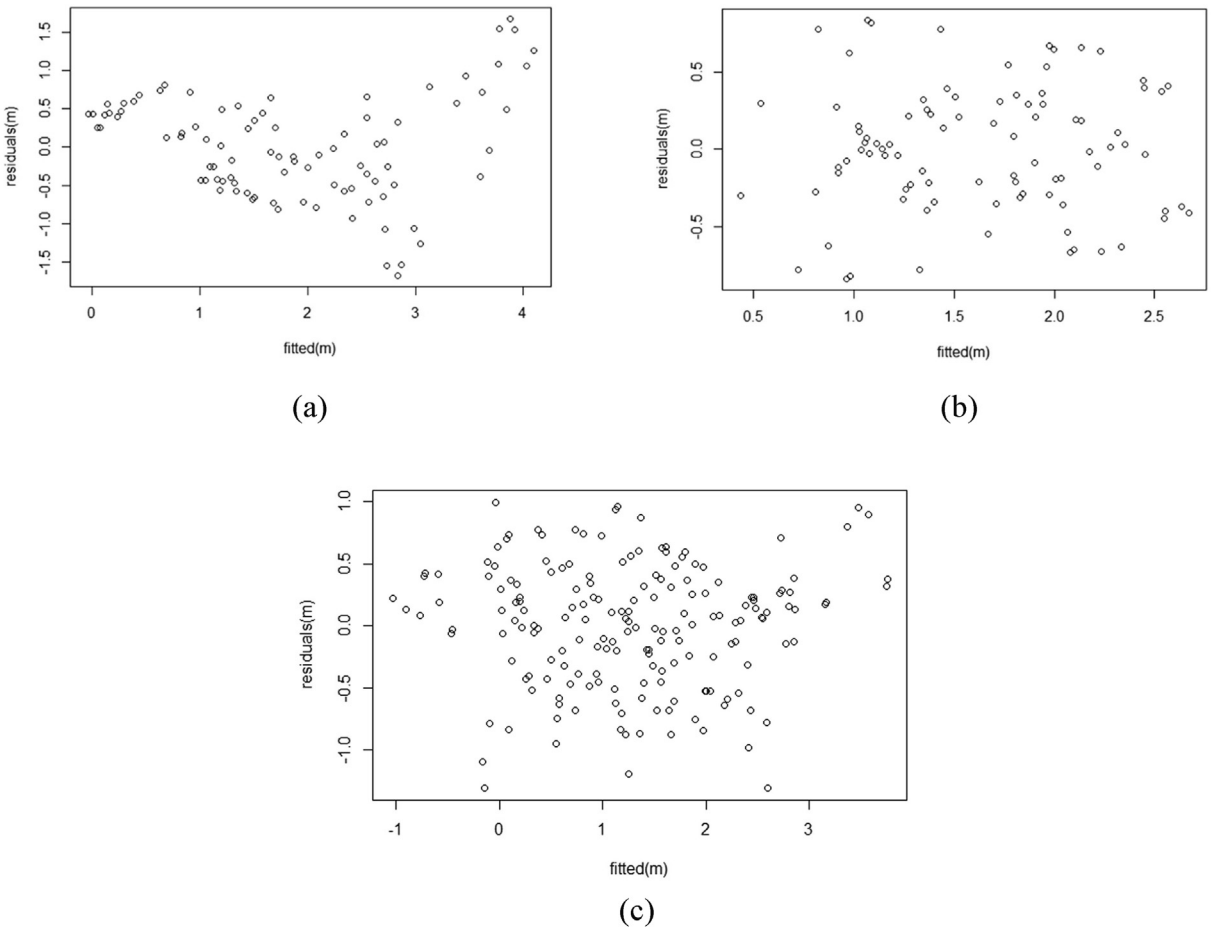

Fig. 18. Fitted vs residual values for groups (a) 1, (b) 2 and (c) 3 – Specimen A.

midspan, where the first cracks appeared. However, it is clear that yielding initiated during the third loading stage.

4.2.2. Slope-based RMSD index

As we did in the previous beam analysis, we will firstly study the evolution of the RMSD index from one loading state to another for each sensor. This analysis is focused on the slope-based RMSD index, which links the evolution of the RMSD with the severity of the changes. The procedure followed in this section is analogous to the one we implemented on the first beam. Fig. 23 shows the RMSD values for all sensors together with the fitted straight line.

As it can be observed, the RMSD index at loading state 1 is significantly lower than for the rest of states, which demonstrates the sensitivity of the sensors to the changes experienced by the specimen.

This first result confirms the conclusion to which we arrived in the previous beam, which is that the RMSD values show a tendency to increase as the load increases. The fact that this tendency is shown in all sensors gives us a strong indication that all of them have been able to capture the propagation of the changes experienced by the beam. In addition to this, sensors PZT1 and PZT3 show a significantly higher RMSD value compared to the other two sensors, which correlates with the fact that the areas close to sensors PZT1 and PZT3 were subjected to more severe changes. This first analysis brings us to the same two outcomes we arrived to previously; first, all sensors show a clear distinction between the initial state (State 1) and the rest of states, which means that all sensors where able to detect the variations. Second, since the RMSD increases progressively, all sensors have been capable to capture the increasing severity of changes.

On the other hand, another key aspect of this analysis that provides useful information is the slope. The fact that sensors PZT1 and PZT3 present a higher slope indicates that these sensors were subjected to a more severe changes compared to sensors PZT2 and PZT4, which correlates with the experimental results. In addition to this, sensor PZT4 presents a positive slope even though it has an abnormally low RMSD value at damage state 5. This result confirms the robustness of this method to assess the variations despite the presence of anomalous data points.

Internal sensors present a similar behaviour to the previous. Moreover, we noted previously that the potential of this method relies on the fact that single outlying values do not drastically change the conclusions. This can be seen studying sensor PZT8, which presents a positive slope even though the RMSD value for state 4 does not follow the expected trend. Concerning the rest of sensors, all of them point to the same outcomes as we did before.

Another interesting variable of this figure is the slope. As it can be examined, the highest slope corresponds to the sensor that was subjected to the most severe changes (sensor PZT7), which correlates well with the experimental results. In addition, the slope for sensor PZT6 is higher than for the other two sensors, which again points to the fact that the most severe changes were surrounding the right side of the array.

In conclusion, it has been proved that both the RMSD index and the slope-based RMSD are useful tools to assess the changes experienced by the beam. All sensors presented robust indicators that pointed towards the same result, capturing the progressive changes experienced by the specimen. In addition to this, the value of the slopes also gathered meaningful information on the severity of the changes around each sensor.

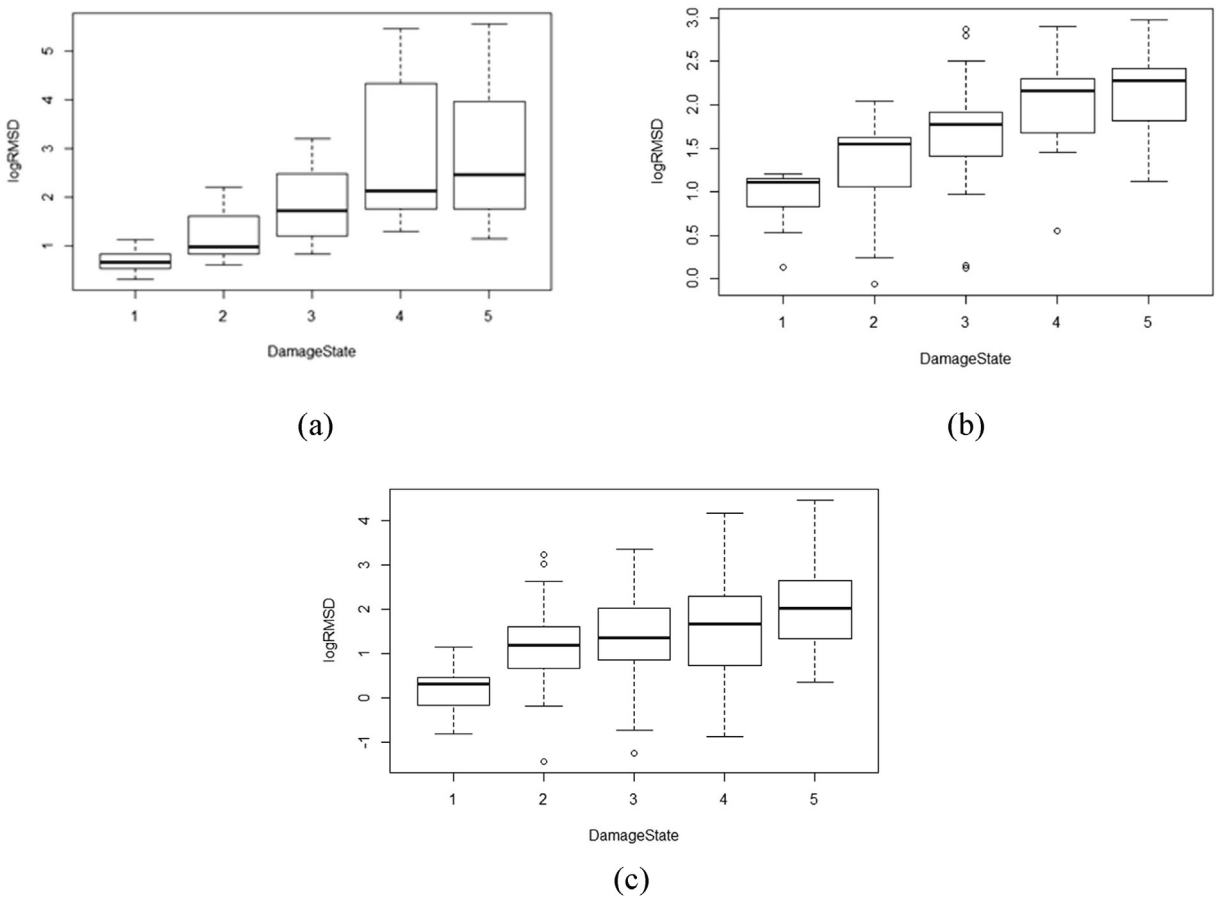

Fig. 19. Boxplots for groups (a) 1, (b) 2 and (c) 3 – Specimen A.

Table 5
Analysis of deviance – Groups of sensors of specimen A.

	p-value		
	Group 1	Group 2	Group 3
Damage	6.81e−9	4.54e−7	2e−16
Frequency	0.6470	0.12328	2e−16
Damage:Frequency	0.9972	0.9888	0.94439

Table 6
Damage states pairwise comparison – Groups of sensors of specimen A.

Damage states	p-value		
	Group 1	Group 2	Group 3
1–2	0.217236	0.251627	7.64e−11
1–3	0.004039	0.007276	4.78e−13
1–4	6.12e−07	1.55e−05	<2e−16
1–5	1.18e−07	2.39e−06	<2e−16
2–3	0.147943	0.251627	0.34094
2–4	0.000116	0.003608	0.01128
2–5	2.39e−05	0.000673	4.99e−09
3–4	0.029211	0.182479	0.09634
3–5	0.008810	0.056902	4.46e−07
4–5	0.607605	0.561941	0.00141

4.2.3. Application of LMM

In this section we will try to answer the same questions that were exposed in the analysis for the previous beam. That is, we will first investigate up to which extent the variation in the RMSD index is due to the loss of structural integrity in the beam. Once this question has been answered, we will analyze how different each of the individual damage states are from each other. This will help us understand if this methodology has been able to capture the progression of the damage in the beam. This analysis will be conducted examining the influence of the type of sensor and the frequency of excitation on the damage detection performance.

This analysis will be carried out using a linear mixed effects model, which was explained in detail in previous sections. In this case, we will work with 4 damage states (2 to 5) since damage state 1 will be used as a baseline for comparison.

We will follow a similar structure as in the previous beam. We will firstly focus on studying the potential influence of the damage state on the RMSD using all the sensors. Once this has been performed, three more analyzes will be carried out, one for each group of sensors: Group 1, which includes sensors PZT1 and PZT2, the larger surface-bonded sensors, group 2 including sensors PZT3 and PZT4, the smaller surface-bonded sensors, and group 3 including sensors PZT6, PZT7, PZT8 and PZT9, which are all embedded sensors of the same type. The objective of performing this analysis split by group is to study how the type and condition of a sensor affects its damage sensitivity. Finally, another analysis will be performed focused on the frequencies, in order to understand which frequencies have more influence on the RMSD or help differentiate between damage states better.

As in the previous analysis performed on beam A, firstly, the conditions presented at the end of Section 3 should be checked. Although not shown here all the procedure again, data do not satisfy all the conditions and we will work with the log-transform of the RMSD indices, which meets suitably the needed requirements. The model will be the same of Eq. (9).

Table 7
Analysis of deviance – Embedded sensors of specimen A.

	p-value			
	PZT6	PZT7	PZT8	PZT9
Damage	4.634e−12	2.180e−6	1.839e−8	8.567e−14

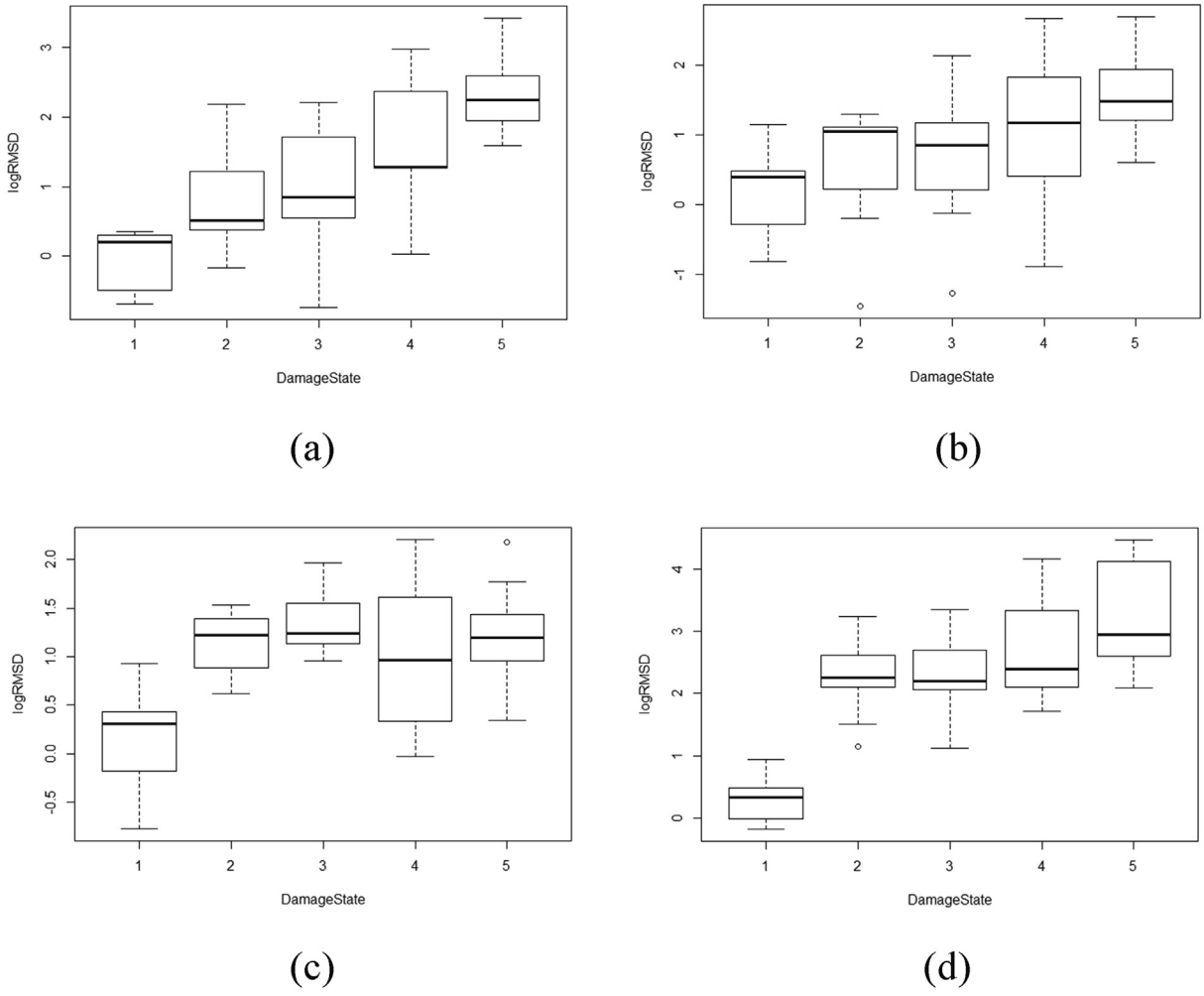

Fig. 20. Boxplots for (a) PZT6, (b) PZT7, (c) PZT8 and (d) PZT9 – Specimen A.

Table 8
Damage states pairwise comparison – Embedded sensors of specimen A.

Damage states	p-value			
	PZT6	PZT7	PZT8	PZT9
1–2	0.001438	0.213493	2.17e−6	9.06e−10
1–3	0.000236	0.158923	2.67e−8	6.52e−10
1–4	4.12e−8	0.000903	2.74e−5	1.03e−11
1–5	2.25e−12	2.31e−6	3.32e−7	6.22e−14
2–3	0.477581	0.634747	0.5321	0.855980
2–4	0.001499	0.062018	1	0.175416
2–5	4.12e−8	0.000255	1	0.000676
3–4	0.006976	0.158923	0.0872	0.175416
3–5	2.32e−7	0.000903	1	0.000950
4–5	0.001438	0.158923	0.5321	0.082212

The analysis of variance (ANOVA) using the F-test performed for model objects produced by LMM gives the results shown in Table 12.

By following the same reasoning used for beam A, three important conclusions can be extracted from this analysis. First, it proves that the damage state has a significant influence on the RMSD, since the p-value for this variable is significantly smaller than 0.05. This is an important conclusion since it has led us to prove that, among all variables, the damage state influences the RMSD significantly, and there-

Table 9
Subfrequency intervals pairwise comparison – Group 3 of sensors of specimen A.

Intervals	p-value	Intervals	p-value	Intervals	p-value
1–2	0.594938	2–7	2.76e−10	4–8	0.004035
1–3	0.991201	2–8	1.25e−12	4–9	1.48e−05
1–4	0.084888	2–9	< 2e−16	5–6	0.495074
1–5	0.428159	3–4	0.991201	5–7	0.009263
1–6	0.001783	3–5	0.991201	5–8	0.000278
1–7	2.69e−06	3–6	0.106100	5–9	5.17e−07
1–8	2.25e−08	3–7	0.000787	6–7	0.934839
1–9	1.14e−11	3–8	1.34e−05	6–8	0.144079
2–3	0.028402	3–9	1.45e−08	6–9	0.002006
2–4	0.000170	4–5	0.991201	7–8	0.991201
2–5	0.002639	4–6	0.991201	7–9	0.188935
2–6	7.56e−07	4–7	0.085189	8–9	0.991201

Table 10
Analysis of deviance – Group 3 of sensors of specimen A.

	p-value	
	Frequency intervals 1 to 5	Frequency intervals 6 to 9
Damage	1.209e−12	4.686e−14
Frequency	0.0001833	0.001062
Damage:Frequency	0.9804853	0.982260

Table 11
Damage states pairwise comparison – Group 3 of sensors of specimen A.

Damage states	p-value	
	Frequency intervals 1 to 5	Frequency intervals 6 to 9
1–2	3.28e−5	3.98e−6
1–3	1.22e−5	6.12e−8
1–4	2.53e−6	3.59e−12
1–5	8.44e−14	2.13e−13
2–3	1	0.520295
2–4	1	0.002232
2–5	4.99e−5	0.000189
3–4	1	0.036480
3–5	0.000123	0.005175
4–5	0.000450	0.520295

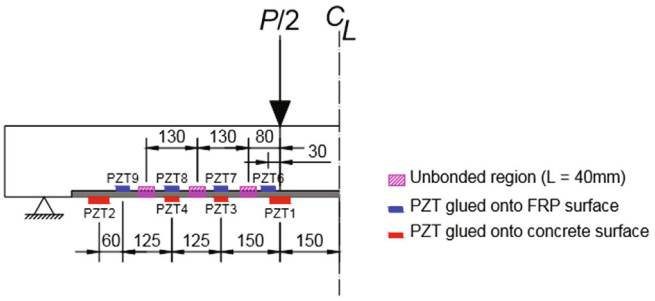

Fig. 21. Experimental layout for the PZT sensors – Specimen B.

fore it is reasonable to use this damage metric to assess the structural condition of the beam. In the same way, this analysis also proves that the frequency interval has a significant influence on the RMSD. Finally, from this analysis we can also conclude that there is no significant interaction between the damage state and the frequency.

This overall analysis allows us to perform a second analysis where we test how different each damage state is from the rest (Table 13). As in previous analyses, p-values lower than 0.05 mean the model has successfully identified between each pair of damage states. Results show the model has identified the difference between states 2–3,

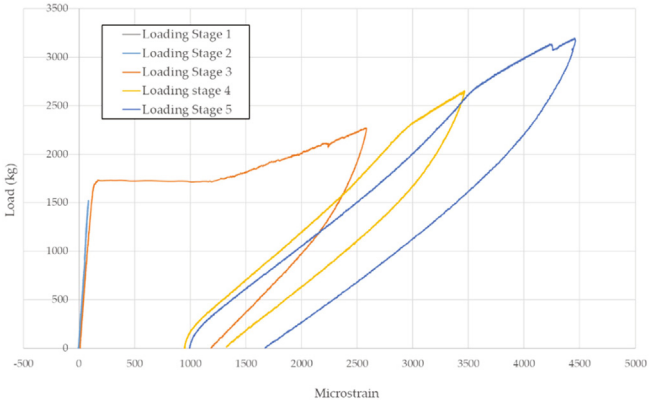

Fig. 22. Experimental load vs microstrain – Specimen B.

2–4, 2–5 and 3–5 with a significant confidence. However, the model has failed to distinguish between damage states 3–4 and 4–5. However, for the successful cases, the performance has been worse than for the previous beam (where there was a significant difference between every pair of damage states). This has been attributed to two factors: first, it is important to remember that the baseline for the calculation of the RMSD is the signal at loading state 1, and not loading state 0 as it was in the first beam. This could have led to the loss of some important information, since the impedance signals are not being compared to the healthy state anymore. Second, since the failure mode was not the expected one, some of the PZT sensors did not provide as much significant information as in the previous beam. This is because they were further away from the damaged area and therefore could not capture its progression as accurately.

Once this overall analysis has been carried out we proceed to perform the same analysis but this time focusing on each group of sensors. We will follow the same structure as in the previous analysis and will work with the log(RMSD) value.

Table 14 shows the results from the variance analysis. As it can be observed, the p-value is much lower than 0.05 for both the damage state variable and for the frequency variable, meaning that both of them have a significant influence on the RMSD for the three groups of sensors. Moreover,

the fact that the damage state affects the damage index significantly means that Group 3 of sensors has been able to capture the presence of damage. This analysis allows us to perform a second analysis where we test how different each damage state is from the rest.

Fig. 24 presents the boxplots for each damage state and group of sensors. As it can be observed, especially for groups 1 and 2, there is a subtle change between some pairs of damage states. However, since some damage states present a high variance, this difference is not clear for all pairs. For group 3 there appears to be a more noticeable change

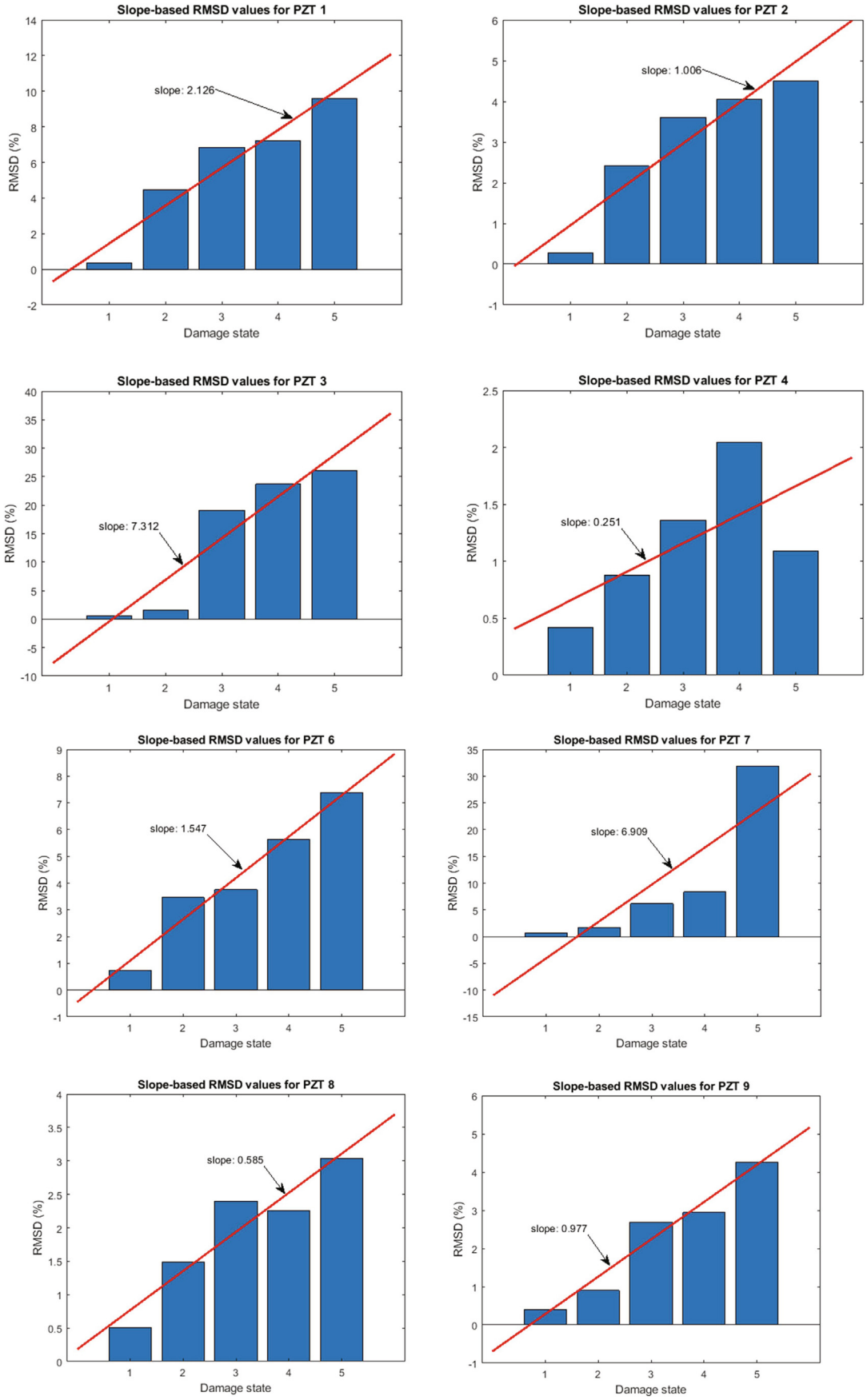

Fig. 23. Slope-based RMSD values – Specimen B.

Table 12
Analysis of deviance – Specimen B.

	Damage state	Frequency	Damage state:frequency
p-value	2.2e−16	2.596e−6	0.9998343

Table 13
Damage states pairwise comparison – Specimen B.

Damage stages	p-value
2–3	5.56e−09
2–4	3.11e−13
2–5	<2e−16
3–4	0.14179
3–5	0.00177
4–5	0.14179

Table 14
Analysis of deviance – Groups of sensors of specimen B.

	p-value		
	Group 1	Group 2	Group 3
Damage	2.236e−06	3.208e−05	<2e−16
Frequency	2.868e−11	0.0001464	3.61e−10
Damage:Frequency	0.6389	0.9998788	0.84311

when we move from one damage state to another. However, we do not have enough information to assess how different the damage states are based solely on this figure. The pairwise analysis will help us understand which pairs of damage states are significantly different from each other.

Table 15 shows the results from the pairwise analysis. As it can be noticed, this first and second group of sensors fail to detect a significant difference between the last steps of the damage scenarios (3 to 5). The only damage step that has showed a significant difference from the rest has been damage step 2 but, even in this case, group 2 leads to worse results than group 1. In general, both, groups 1 and 2, do not show a good performance in detecting the propagation of the damage. Sensors of Group 3 are able to distinguish between almost every pair of damage states. Only for pair 3–4 the p-value is higher than 0.05. On top of this, the performance of sensors of Group 3 alone has been better than in the overall analysis with all the sensors. This can be attributed to the fact that, since Groups 1 and 2 of sensors are unable to differentiate the last damage steps, mixing their data with that of Group 3 adds noise to these last damage steps, making it harder to tell them apart. As a conclusion, it can be stated that the sensors of Group 3 have shown the best performance amongst all groups at detecting the presence and propagation of the damage. In addition, we can infer that

Table 15
Damage states pairwise comparison – Groups of sensors of specimen B.

Damage stages	p-value		
	Group 1	Group 2	Group 3
2–3	0.000287	0.001745	1.01e−06
2–4	1.35e−05	5.79e−05	4.11e−09
2–5	7.55e−06	0.000245	< 2e−16
3–4	0.569810	0.622633	0.218153
3–5	0.568954	0.923506	1.08e−05
4–5	0.802810	0.923506	0.000812

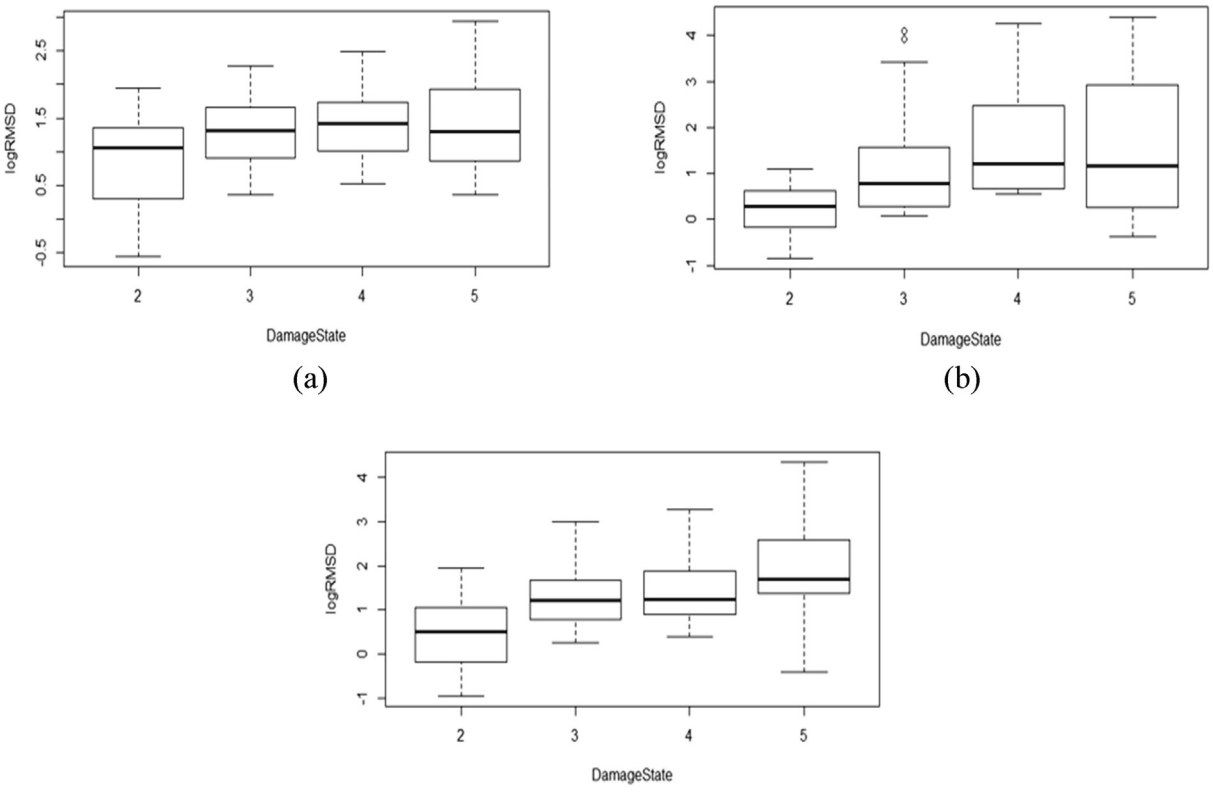

Fig. 24. Boxplots for groups (a) 1, (b) 2 and (c) 3 – Specimen B.

Table 16
Analysis of deviance – Embedded sensors of specimen B.

	p-value			
	PZT6	PZT7	PZT8	PZT9
Damage	0.006236	2.179e−8	0.004751	9.842e−10

Table 17
Damage states pairwise comparison – Embedded sensors of specimen B.

Damage states	p-value			
	PZT6	PZT7	PZT8	PZT9
2–3	0.8978	0.000457	0.02394	5.5e−7
2–4	0.0587	6.35e−5	0.08015	1.91e−7
2–5	0.0142	7.21e−9	0.00461	6.52e−10
3–4	0.1544	0.336346	0.93045	0.57582
3–5	0.0474	0.000143	0.93045	0.00634
4–5	0.8978	0.000864	0.55996	0.01657

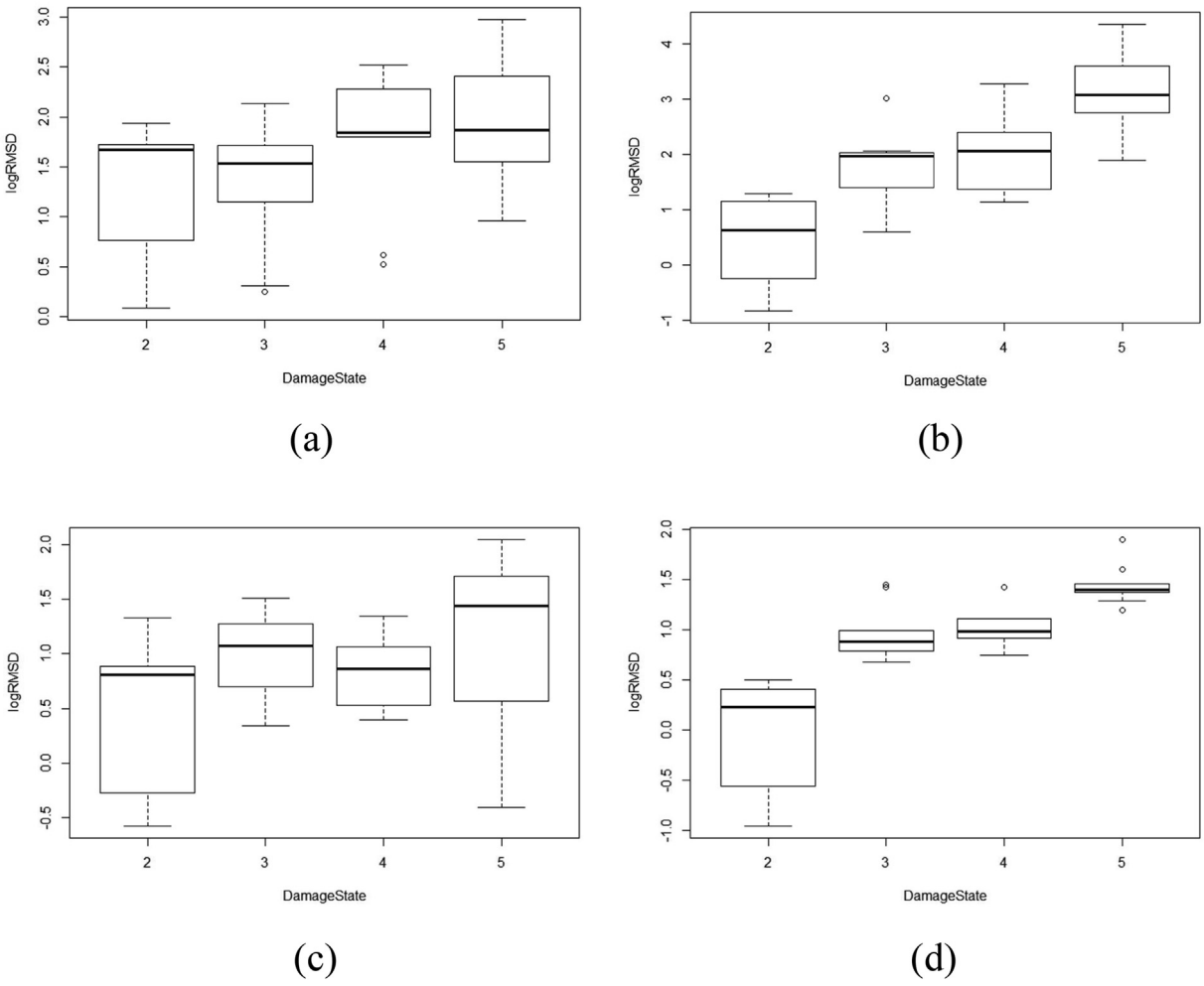

Fig. 25. Boxplots for (a) PZT6, (b) PZT7, (c) PZT8 and (d) PZT9 – Specimen B.

this group of sensors is the one that contributes the most to the sensitivity to damage of the complete array of 8 sensors.

According to the previous results, the study was focused subsequently on sensors belonging to group 3. Tables 16 and 17 and Fig. 25 show the p-value for the damage from the variance analysis, the boxplots and the damage states pairwise comparison, respectively. For this specimen, even although an unexpected failure by rupture of FRP occurred, a large crack on the right of sensor PZT7 overlapping

with the closest debonded area to the midspan was identified after failure. This might be an indication that the loss of adherence around the area surrounding sensor PZT7 was near as Fig. 25 and Table 17 show.

For this specimen, a final analysis focused on the dependence on the sub-frequency intervals was also carried out for group 3 of sensors. However, for simplicity, the results are not presented here since the conclusions are the same than for specimen A, the frequencies did not play a major role in the damage detection capability of Group 3 of sensors.

5. Conclusions

This paper develops a procedure for damage identification of structural concrete members rehabilitated by NSM FRP systems. The procedure is based on the implementation of linear mixed methods in combination with EMI results captured from piezoelectric sensors bonded on the analyzed beam. The performance evaluation of the proposed approach has been made with two experimental tests on concrete beams strengthened with NSM-FRP.

Once their assumptions have been checked, LMMs, as an approach for spatial linear model selection applicable to classified spatial data, allow to incorporate the spatial information provided by the different sensors into a data model and a classification rule specification, from which an analysis of the data is performed. It makes them compare favourably against other selection approaches.

With the proposed methodology, various problems to be solved in the application of EMI technique to achieve the ultimate goal of locating and identifying damage have been addressed in a fast and reliable way. These problems include the use of an efficient statistical metrics sensitive enough to damage, the importance or not of selecting a suitable frequency range and the need to filter the random or uncontrollable phenomena typical from experimental tests. One of the trends of this study is that LMMs, whose use is increasing everyday in other areas, has allowed to address for the first time all these aspects in a direct way. Moreover, another topic to be covered in the future, the compensation of environmental factors such as temperature variations, might also be dealt with this methodology.

6. Data availability statement

The raw/processed data required to reproduce these findings cannot be shared at this time, as the data also forms part of an ongoing study.

Declaration of Competing Interest

The authors declare that they have no known competing financial interests or personal relationships that could have appeared to influence the work reported in this paper.

Acknowledgements

The writers acknowledge the support for the work reported in this paper from the Spanish Ministry of Science, Innovation, and Universities (projects BIA2017-84975-C2-1-P and BIA2017-84975-C2-2-P).

References

[1] Teng JG, Chen JF, Smith ST, Lam L. CFRP strengthened RC structures. 1st Ed. West Sussex: John Wiley and Sons; 2002.
[2] Bank LC. Composites for construction: structural design with CFRP materials. 1st Ed. West Sussex: John Wiley and Sons; 2006.
[3] Balaguru P, Nanni A, Giancaspro J. CFRP composites for reinforced and prestressed concrete structures. A guide to fundamentals and design for repair and retrofit. New York and London: Taylor and Francis; 2009.
[4] Al-Mahmoud F, Castel A, François R, Tourneur C. RC beams strengthened with *NSM* CFRP rods and modeling of peeling-off failure. Compos Struct 2010;92(8):1920–30.
[5] Al-Saadi NTK, Mohammed A, Al-Mahaidi R, Sanjayan J. State-of-the-art review: Near-surface mounted FRP composites for reinforced concrete structures. Constr Building Mater 2019;209:748–69.
[6] Abdallah M, Al Mahmoud F, Khelil A, Mercier J, Almassri B. Assessment of the flexural behavior of continuous RC beams strengthened with NSM-FRP bars, experimental and analytical study. Compos Struct 2020;242:112127. https://doi.org/10.1016/j.compstruct.2020.112127.
[7] Doebling SW, Farrar CR, Prime MB. A summary review of vibration-based damage identification methods. Shock Vib Dig 1998;30(2):91–105.
[8] Sevillano E, Sun R, Perera R. Damage evaluation of structures with uncertain parameters via interval analysis and FE model updating methods. Struct Control Health Monit 2017;24(4):e1901. https://doi.org/10.1002/stc.v24.410.1002/stc.1901.
[9] Perera R, Sandercock S, Carnicero A. Civil structure condition assessment by a two-stage FE model update based on neural network enhanced power mode shapes and an adaptive roaming damage method. Eng Struct 2020;207:110234. https://doi.org/10.1016/j.engstruct.2020.110234.
[10] Capozucca R, Domizi J, Magagnini E. Damaged RC beams strengthened with NSM CFRP rectangular rods under vibration in different constrain conditions. Compos Struct 2016;154:660–83.
[11] Sevillano E, Sun R, Gil A, Perera R. Interfacial crack-induced debonding identification in FRP strengthened RC beams from PZT signatures using hierarchical clustering analysis. Compos Part B Eng 2016;87:322–35.
[12] Na W, Baek J. A review of the piezoelectric electromechanical impedance based structural health monitoring technique for engineering structures. Sensors 2018;18(5):1307. https://doi.org/10.3390/s18051307.
[13] Zhu J, Qing X, Liu X, Wang Y. Electromechanical impedance-based damage localization with novel signatures extraction methodology and modified probability-weighted algorithm. Mech Syst Signal Pr 2021;146:107001. https://doi.org/10.1016/j.ymssp.2020.107001.
[14] Malinowski PH, Wandowski T, Singh SK. Employing principal component analysis for assessment of damage in GFRP composites using electromechanical impedance. Compos Struct 2021;266:113820. https://doi.org/10.1016/j.compstruct.2021.113820.
[15] Perera R, Pérez A, García-Diéguez M, Zapico-Valle J. Active wireless system for structural health monitoring applications. Sensors 2017;17(12):2880. https://doi.org/10.3390/s17122880.
[16] West BT, Welch KB, Galecki AT. Linear Mixed Models: A Practical Guide Using Statistical Software. Second Edition. Taylor & Francis; 2014.
[17] Winter B. Linear models and linear mixed effects models in R with linguistic applications. Merced, Cognitive and Information Sciences: University of California; 2016.
[18] Meteyard L, Davies RAI. Best practice guidance for linear mixed-effects models in psychological science. J Mem Lang 2020;112:104092. https://doi.org/10.1016/j.jml.2020.104092.
[19] Graves CE, McManus CM, Chabot JA, Lee JA, Kuo JH. Vitamin D does not affect intraoperative parathyroid hormone kinetics: A mixed linear model analysis. J Surg Res 2019;241:199–204.
[20] Wang G, Aschenbrenner AJ, Li Y, McDade E, Liu L, Benzinger TLS, et al. Two-period linear mixed effects models to analyze clinical trials with run-in data when the primary outcome is continuous: Applications to Alzheimer's disease. Alzheimers Dement (N Y) 2019;5(1):450–7.
[21] Dreiziene L, Ducinskas K. Comparison of spatial linear mixed models for ecological data based on the correct classification rates. Spat Stat 2020;35:100395. https://doi.org/10.1016/j.spasta.2019.100395.
[22] Perera R, Torres L, Ruiz A, Barris C, Baena M. An EMI-based clustering for structural health monitoring of NSM FRP strengthening systems. Sensors 2019;19(17):3775.
[23] Liang C, Sun FP, Rogers CA. Electro-mechanical impedance modeling of active material systems. J Intell Mater Syst Struct 1994;21(3):232–52.
[24] Xu D, Huang S, Cheng X. Electromechanical impedance spectra investigation of impedance-based PZT and cement/polymer based piezoelectric composite sensors. Constr Build Mater 2014;65:543–50.
[25] Bhalla SK, Moharana S. Modelling of piezo-bond structure system for structural health monitoring using EMI technique. Key Eng Mater 2013;569:1234–40.
[26] Giurgiutiu V, Zagrai A. Damage detection in thin plates and aerospace structures with the electro-mechanical impedance method. Struct Health Monit 2005;4(2):99–118.
[27] Park G, Inman DJ. In: Damage Prognosis: For Aerospace, Civil and Mechanical Systems. Chichester, UK: John Wiley & Sons, Ltd; 2005. p. 275–92. https://doi.org/10.1002/0470869097.ch13.
[28] RStudio Desktop (2019). RStudio: Integrated Development for R.RStudio, Inc., Boston, MA URL http://www.rstudio.com/.
[29] Ai D, Zhu H, Luo H. Sensitivity of embedded active PZT sensor for concrete structural impact damage detection. Constr Build Mater 2016;111:348–57.
[30] Yang Y, Divsholi BS. Sub-frequency interval approach in electromechanical impedance technique for concrete structure health monitoring. Sensors 2010;10(12):11644–61.